This is a preprint, the final version is subject to change, of the American Mineralogist (MSA)
Cite as Authors (Year) Title. American Mineralogist, in press.
DOI: https://doi.org/10.2138/am-2018-6319

Revision 1.0

Accurate Predictions of Microscale Oxygen Barometry in Basaltic Glasses Using Vanadium K-edge X-ray Absorption Spectroscopy: A Multivariate Approach

ANTONIO LANZIROTTI[1,*], M. DARBY DYAR[2,3], STEPHEN SUTTON[1], MATTHEW NEWVILLE[1], ELISABET HEAD[4], CJ CAREY[5], MOLLY MCCANTA[6], LOPAKA LEE[7], PENELOPE L. KING[8], AND JOHN JONES[9]

[1] Center for Advanced Radiation Sources, The University of Chicago, Argonne, IL 60439, USA

[2] Department of Astronomy, Mount Holyoke College, South Hadley, MA 01075, USA

[3] Planetary Science Institute, 1700 E. Fort Lowell, Tucson, AZ 85719, USA

[4] Department of Earth Science, Northeastern Illinois University, Chicago, IL 60625, USA

[5] College of Information and Computer Sciences, University of Massachusetts, Amherst, MA 01003, USA

[6] Department of Earth and Planetary Sciences, University of Tennessee, Knoxville, TN 37996, USA

[7] US Geological Survey, Hawaii Volcano Observatory, MS964, Hawaii National Park, HI 96718, USA

[8] Research School of Earth Sciences, Australian National University, Canberra, ACT 2601, Australia

[9] National Aeronautics and Space Administration/Johnson Space Center, Houston, TX 77058, USA

ABSTRACT

Because magmatic oxygen fugacity (fO_2) exerts a primary control on the discrete vanadium (V) valence states that will exist in quenched melts, V valence proxies for fO_2, measured using X-ray absorption near-edge spectroscopy (XANES), can provide highly sensitive measurements of the redox conditions in basaltic melts. However, published calibrations for basaltic glasses primarily relate measured intensities of specific spectral features to V valence or oxygen fugacity. These models have not exploited information contained within the entire XANES spectrum, which also provide a measure of changes in V chemical state as a function of fO_2. Multivariate analysis (MVA) holds significant promise for the development of calibration models that employ the full XANES spectral range. In this study, new calibration models are developed using MVA partial

least-squares (PLS) regression and least absolute shrinkage and selection operator (Lasso) regression to predict the fO_2 of equilibration in glasses of basaltic composition directly. The models are then tested on a suite of natural glasses from mid-ocean ridge basalts and from Kilauea. The models relate the measured XANES spectral features directly to buffer-relative fO_2 as the predicted variable, avoiding the need for an external measure of the V valence in the experimental glasses used to train the models. It is also shown that by predicting buffer-relative fO_2 directly, these models also minimize temperature-relative uncertainties in the calibration. The calibration developed using the Lasso regression model, using a Lasso hyperparameter value of $\alpha = 0.0008$, yields NNO relative fO_2 predictions with a root-mean-square-error of ±0.33 log units. When applied to natural basaltic glasses, the V MVA calibration model generally yields predicted NNO-relative fO_2 values that are within analytical uncertainty of what is calculated using Fe XANES to predict $Fe^{3+}/\Sigma Fe$. When applied to samples of natural basaltic glass collected in 2014 from an active lava flow at Kilauea, a mean fO_2 of NNO-1.15 ±0.19 (1σ) is calculated, which is generally consistent with other published fO_2 estimates for subaerial Kilauea lavas. When applied to a sample of pillow-rim basaltic glass dredged from the East Pacific Rise, calculated fO_2 varies from NNO-2.67 (±0.33) to NNO-3.72 (±0.33) with distance from the quenched pillow rim. Fe oxybarometry in this sample provides an fO_2 of NNO-2.54 ±0.19 (1σ), which is in good agreement with that provided by the V oxybarometry within the uncertainties of the modeling. However, the data may indicate that V XANES oxybarometry has greater sensitivity to small changes in fO_2 at these more reduced redox conditions than can be detected using Fe XANES.

Keywords: XANES, vanadium, valence, oxygen fugacity, basalts, multivariate analysis

This is a preprint, the final version is subject to change, of the American Mineralogist (MSA)
Cite as Authors (Year) Title. American Mineralogist, in press.
DOI: https://doi.org/10.2138/am-2018-6319

Revision 1.0

INTRODUCTION

Accurate estimates of the intrinsic oxygen fugacity (fO_2) of magmas are important for constraining source composition and understanding the conditions under which melts are generated, their sub-liquidus evolution and crystallization history, and the composition and evolution of volcanic gases released to the atmosphere (i.e. Sato 1978; Mathez 1984; Christie et al. 1986; Ballhaus et al. 1990; Carmichael 1991; Kelley and Cottrell 2009). Glasses from mantle-derived basaltic melts have the potential to provide a record of the fO_2 at equilibration. Volcanic and magmatic glasses should closely approximate the composition of the quenched liquid, and thus generally be free of the complexities that can arise in estimating fO_2 based on analysis of crystalline samples of basalt, where the effects of mineral-melt partitioning need to be accounted for.

Analytical measurements of the $Fe^{3+}/\Sigma Fe$ ratio in volcanic glasses and melt inclusions are commonly used to constrain melt fO_2 (Christie et al. 1986; Bézos and Humler 2005; Cottrell and Kelley 2011; Zhang et al. 2016). The oxidation state of iron (Fe), typically the most abundant heterovalent element in basaltic liquids, is the easiest of the multivalent elements to measure and is generally considered to most directly reflect the melt's fO_2 at equilibration. X-ray absorption near edge structure (XANES) spectroscopy at the Fe K-edge has been shown to generally provide precise and accurate measures of $Fe^{3+}/\Sigma Fe$ ratios in terrestrial basaltic glasses (Berry et al. 2003; Cottrell et al. 2009; de Moor et al. 2013; Dyar et al. 2016a). XANES is one of the few methods capable of determining elemental valence state in small, micrometer size melt inclusions or valence-state partitioning of elements between crystals and glasses in micrometer-scale experiments (e.g., King et al. 2000). However, Fe XANES calibrations in basaltic systems become less sensitive when measuring $Fe^{3+}/\Sigma Fe$ ratios less than ~0.09 (Cottrell and Kelley

2011), with correspondingly higher uncertainties. This is particularly true for calibrations based on measuring pre-edge peak intensities because crystal field effects, orbital mixing, and site distortions common to XANES spectra from glasses make it more difficult to detect relative changes in intensities at the reduced end-member composition. This limitation is especially important because published estimates for the average $Fe^{3+}/\Sigma Fe$ ratio of the most common terrestrial extrusive igneous rocks, mid-ocean ridge basalts (MORB), range from ~0.08 and 0.16 (Christie et al. 1986; Bézos and Humler 2005; Cottrell and Kelley 2011). Our ability to constrain the fO_2 values of terrestrial and extraterrestrial basaltic sources hinges on accurate methods for determining fO_2 in reduced systems where Fe XANES is becoming insensitive.

Here we explore a refined calibration of the vanadium (V) valence state oxybarometer for basaltic glasses, using multivariate analysis (MVA) modeling of V K-edge XANES spectra. For terrestrial basalts, V XANES oxybarometry is expected to provide generally similar estimates of the fO_2 equilibration conditions of a melt to estimates based on Fe oxidation state measurements. However, an advantage in using V XANES oxybarometry is that its valence varies continuously from V^{3+} to V^{5+} over a wider range of fO_2 than Fe^{2+} to Fe^{3+}, making V potentially a more sensitive proxy in low-fO_2 systems where $Fe^{3+}/\Sigma Fe$ ratios are typically <0.1, conditions where many terrestrial and extraterrestrial basaltic melts are generated.

In the fO_2 range where terrestrial basalts are generated, V valence varies from V^{3+} to V^{5+}, with V^{4+} dominant near the quartz-fayalite-magnetite (QFM) redox buffer (Papike et al. 2005). The $V^{3+} \leftrightarrow V^{4+}$ and $V^{4+} \leftrightarrow V^{5+}$ multivalent couples will span an oxygen fugacity range relative to the nickel-nickel oxide (NNO) buffer from about NNO-6 to NNO+3.5 (Papike et al. 2005) in basaltic melts. Magma fO_2 exerts the primary control on the discrete V valence states that will exist in the quenched liquid (Canil 1997, 1999; Canil and Fedortchouk 2001; Giuli et al. 2004;

Papike et al. 2005; Mallmann and O'Neill 2009). Sutton et al. (2005) developed a fO_2 calibration model based on the intensity of the V XANES pre-edge peak measured in experimental glasses produced at known fO_2 and temperature (T) under isobaric conditions. This fO_2 calibration is relatively simple to apply (Sutton et al. 2005; Karner et al. 2006; Righter et al. 2011). However, by using only the pre-edge peaks it does not exploit potentially sensitive information about vanadium's chemical state contained in the entire spectrum (Fig. 1), including the energy and structure of the rising absorption edge, the white line, and potentially extending into the higher energy, fine structure region of the absorption spectra (the EXAFS region). In quenched glasses, these higher energy parts of the spectra provide an additional measure of V speciation and coordination, and how these change in response to changing redox conditions of the melt. By exploiting the full range of the XANES spectrum, it may be possible to develop a calibration with improved precision and accuracy over a broader range of fO_2.

Multivariate analysis holds significant promise for the development of calibration models that use the full spectral range. Recently, such MVA modeling has been applied to Fe XANES collected from both glasses and minerals to improve the accuracy of predicting $Fe^{3+}/\Sigma Fe$ (Dyar et al. 2016a, 2016b). In these studies, two MVA approaches were explored, partial least-squares regression (PLS) and least absolute shrinkage and selection operator (Lasso). In the present study, these methods have been applied to V XANES spectra collected for experimental and natural basaltic glasses using the entire measured spectra rather than the intensity or energy position of a specific spectral feature. The large differences observed in the energy and intensity of V XANES spectral structures for glasses equilibrated over a broad range of fO_2 conditions make them highly suited to MVA. The spectral differences for basaltic glasses primarily reflect changes in the effective V valence (V*) and differences in multiple scattering resonances of the

photoelectrons by the neighbor oxygen atoms. In terrestrial basalts, it is convenient to define V* (Sutton et al. 2005) as the respective fractional contribution of V^{3+}, V^{4+} and V^{5+} in the system.

An advantage of MVA is that it requires only that the spectra contain information about the variable of interest, there is no need to directly assign spectral features to the underlying fundamental processes. This makes MVA well-suited for applications such as X-ray absorption spectroscopy, where it is often difficult to assign observed spectral features to a unique physical processes within the energy resolution of the measurement. Thus, the study here also explores the potential for generating an accurate oxybarometric MVA calibration model that relates the measured V XANES spectra to predicted oxygen fugacity directly. Existing Fe valence state oxybarometers for basaltic glasses generally relate the XANES spectroscopic features measured in experimental glasses to the $Fe^{3+}/\Sigma Fe$ ratio measured using Mössbauer spectroscopy (Cottrell et al. 2009; Dyar et al. 2016a). The measured Fe valence can then be related to fO_2 through composition-dependent expressions that relate fO_2 to the Fe^{3+}/ Fe^{2+} ratio (Kilinc et al. 1983; Kress and Carmichael 1991). This type of wet chemical determination of the V valence is difficult to do for glasses where the starting materials consist of natural basalt because V concentrations are generally less than 400 ppm. A calibration based on an MVA model that directly relates the measured V XANES spectra to predicted oxygen fugacity increases the number of glasses that can be used in training the calibration model, because the equilibrium redox conditions are always constrained and measured in glass synthesis experiments.

There are, however, important assumptions in the approach presented in this study that need to be evaluated and discussed. Although the calibration presented here is restricted to basaltic glasses, there is an inherent assumption that the measured V speciation does not have a strong compositional dependence for the range of compositions used in building the model. A second

This is a preprint, the final version is subject to change, of the American Mineralogist (MSA)
Cite as Authors (Year) Title. American Mineralogist, in press.
DOI: https://doi.org/10.2138/am-2018-6319

important assumption is that the reaction enthalpy of the buffer the model is calibrated against (in this case nickel-nickel oxide) generally parallels the reduction enthalpies for the V redox couples. The data presented here also provide some initial insights into the potential validity of these assumptions. The MVA models developed are then applied to a suite of natural, basaltic glasses to predict the fO_2 at which they were equilibrated.

SAMPLES AND ANALYTICAL PROCEDURES

Experimental Samples Studied

Three suites of experimental glasses (28 samples in total) were analyzed by V K-edge XANES to build the MVA calibration models. These glasses were equilibrated under varying fO_2 conditions, covering a redox range relative to the nickel-nickel oxide (NNO) buffer from NNO-8.1 to NNO+4.7. Details regarding starting materials, glass compositions, and equilibration conditions under which these glasses were produced can be found in the respective references (indicated below) and are summarized here in Table 1. Both the Cottrell et al. (2009) suite (NMNH 117393) and the Dufresne et al. (2009) suite were synthesized from natural basaltic starting materials at 1 atm pressure. The Cottrell suite basalts were equilibrated at 1350°C in a CO_2-CO atmosphere (log fO_2 -10.19 to -2.20) and mounted for XANES analysis as free-standing, doubly polished glass chips. The Dufresne suite were calibrated at temperatures between 1410-1417°C in either air or CO_2-CO atmosphere (log fO_2 -8.70 to -0.68, verified by a zirconia electrode) and were mounted on a range of noble metal loops (Pt, Pt-Fe and Re). The analyzed Dufresne suite glasses were prepared as polished, epoxy-embedded chips. Vanadium abundances have not been reported for these two suites of glasses, but the starting materials used generally have V concentrations between ~200-300 ppm, typical for natural basaltic glasses. The

$Fe^{3+}/\Sigma Fe$ ratio of both suites of glasses have been measured previously by both Mössbauer and XANES spectroscopy. FeO_T concentrations in the Cottrell suite starting materials range from 9.5-10.2 wt% and in the Dufresne suite from 6.9-14.4 wt%.

Glasses in the Hanson and Jones (1998) suite have forsterite-anorthite-diopside (FAD) compositions doped to provide V concentrations of ~ 3000 ppm. These were also synthesized at 1 atm at equilibration temperatures of 1310 - 1320°C (log fO_2 -15.5 to -4.55). For these glasses, the compositions were synthesized from reagent-grade oxide powders as Fe-free experimental glasses. However, they do contain low abundances of Fe suitable to produce high-quality Fe K-edge XANES for comparison with the measured V XANES data. The Fe in these glasses likely originates from Fe contamination of the Pt loops used in the experiments or in the furnace (Hanson and Jones 1998). We assume the trace Fe measured in the glasses would have been in equilibrium with the melt at quenching. The Hanson and Jones suite analyzed by XANES were prepared as polished, epoxy embedded chips. The uncertainties on measured fO_2 for the Dufresne and Hanson and Jones suite of glasses are assumed to be on the order of 0.1-0.2 log units, since these controlled laboratory redox experiments used Y-doped zirconia cells to verify the fO_2 (Jurewicz et al. 1993).

Natural Samples Studied

The MVA oxybarometer models, trained on the synthetic glasses, were then used to predict the fO_2 of several natural basaltic glass samples (Tables 3, 4, 5). Three are glasses commonly used as microprobe standards (Table 3): U.S. Geological Survey (USGS) basalt glass designated as BCR-2G (Wilson and Taggart 2000) and two microbeam standards from the Smithsonian Institution NMNH National Rock Collection designated A-99 (NMNH 113498-1) and VG-2 (NMNH 111240-52) (Jarosewich et al. 1980). USGS BCR-2G glass was prepared by melting

aliquots of powdered Columbia River basalt standard BCR-2 at 1540°C under a nitrogen atmosphere (Wilson and Taggart 2000). As such, there is little information for what the likely oxygen fugacity may have been at equilibration for this glass, but our analysis should be useful with regard to future studies given the availability of this material. The NMNH standard A-99 consists of samples of fresh basaltic glass collected from the Makaopuhi Lava Lake, Hawaii. NMNH VG-2 consists of samples of fresh basaltic glass dredged from the Juan de Fuca Ridge. All three standard glasses were mounted in epoxy and singly polished to a nominal thickness of ~ 100 μm.

Vanadium and Fe XANES were also measured from a sequence of seven basaltic glasses collected in December, 2014 from an active lava flow at Kilauea (Hawaii) that started in the upper east rift zone near Pahoa, designated sequence J27 (June 27 flow field) by the Hawaii Volcano Observatory (HVO), USGS (Table 4). Lava from this flow is thought to have originated from the shallow magma chamber below Pu'u O'o during the entire duration of the sampling. The flow was traveling through a tube system along its entire axis and seven samples were collected at active breakouts various distances downflow (between 3.4 and 18.7 km) near the central tube. Temperature of the lava melt, as inferred from MgO glass-thermometry (Helz and Thornber 1987), decreased from approximately 1140°C at the vent to 1130°C at the distal flow front 19.2 km away. Additional sampling and compositional details are provided in Table 4. These glasses were mounted in epoxy and singly polished to a nominal thickness of 100 μm. Samples were imaged by optical petrography, by scanning electron microscopy (SEM) and by synchrotron XRF compositional imaging prior to XANES analysis to ensure no microcrystals contributed to the spectroscopic analyses. SEM imaging was conducted at the Scanning Electron Microscope Facility at University of Hawaii at Hilo using a Hitachi S-3400N-II instrument.

Also analyzed in this study is a sample of pillow-rim basaltic glass dredged from the East Pacific Rise (Table 5, sample location between ~ 9°46'N and 9°57'N, Fornari et al. 2012). The sample was sectioned perpendicular to the glassy outer margin through to where the variolitic zone of the pillow begins to be visible (Marescotti et al. 2000) as a 30 μm polished thin section on nominally V-free quartz glass. We define the variolitic zone similarly to how it has been described by Marescotti et al. (2000), recognized by the presence of scattered anisotropic mineral ovoids within isotropic glass. Prior to XANES analysis, the sample was imaged in both reflected and transmitted plane-polarized and cross-polarized light and by synchrotron XRF compositional imaging. A set of V and Fe XANES spectra are presented, collected in pillow glassy rim material extending in to the variolitic zone.

Analytical Methods

Vanadium K-edge XANES spectra were measured using the 13-ID-E undulator-based microprobe at the GeoSoilEnviro-CARS sector, Advanced Photon Source (APS), Argonne National Laboratory, USA. The optical and instrumental configuration of the beamline are described in Lanzirotti et al. (2016) and Sutton et al. (2017). Monochromatic radiation was provided by a cryogenically-cooled double-crystal monochromator using a Si(111) monochromator crystal set delivering an incident flux of ~1.0e^{11} photons/second. Beam focusing to the sample is provided by a pair of 240 mm long, highly polished, silicon mirrors in a Kirkpatrick-Baez (KB) geometry capable of generating focused spot sizes of ~2 μm in the horizontal by ~1 μm in the vertical (FWHM). This spot size was used for XANES analysis of the sample of East Pacific Rise pillow glass, which allowed for spatially resolved X-ray fluorescence compositional mapping of the sample prior to XANES analysis, thus minimizing any potential analysis of micro-inclusions that were not visible optically. The Kilauea glass samples were also

compositionally imaged prior to XANES analysis. However, the XANES analysis of the Kilauea glasses, experimental glasses, and microprobe standard glasses were carried out using a defocused spot size of ~30 × 30 μm in order to minimize the potential for beam induced changes in V valence. Experimental data collected on Kilauea basaltic glass confirms that at these delivered flux densities (photons/sec/μm^2), no change in V speciation is detectable as a function of incident dose. Measured spectra were normalized to incident intensity (I_0) measured in a helium-filled, 200 mm-long ion chamber just upstream of the KB mirror optics. The 1/e absorption depth for V at the K-edge in average basaltic glass is predicted to be ~ 19 μm.

All V XANES spectra were collected in fluorescence mode using a four-element, silicon-drift-diode detector array (Vortex-ME4, Hitachi High-Technologies Science America, Inc.) with pulse-processing provided by an Xspress 3 digital X-ray processor system (Quantum Detectors). The V XANES data were corrected for detector dead time. V K-edge spectra were collected by scanning the incident beam from 5365-5455 eV in 2.5 eV steps, from 5455-5490 eV in 0.2 eV steps, and from 5490-5645 eV in 2.0 eV steps at 6 seconds per energy point. These scan parameters provide 331 measured intensities at 331 energy values which will define the observable variables of the model. The energy of the first derivative peak of V metal foil provided a V K-edge energy of 5463.76 eV, consistent with values determined by Kraft et al. (1996).

For the natural samples and for the Hanson and Jones suite of experimental glasses, Fe K-edge XANES were also collected for comparison with the V spectra. For Fe K-edge spectroscopy, a Si(311) monochromator crystal set was used for optimal energy resolution, delivering an incident flux of ~4.0e^{10} photons/second; also purposely lowered from the maximum possible to reduce the potential for beam-induced changes in Fe valence state. Fe K-

This is a preprint, the final version is subject to change, of the American Mineralogist (MSA)
Cite as Authors (Year) Title. American Mineralogist, in press.
DOI: https://doi.org/10.2138/am-2018-6319

edge XANES were collected by scanning the incident beam from 7012-7102 eV in 6 eV steps, from 7102-7142 eV in 0.1 eV steps, and from 7142-7352 eV in 0.2 eV steps at 0.5 seconds per energy point. For Fe XANES the energy of the first derivative peak of Fe metal foil provided an Fe K-edge energy of 7110.75 eV, consistent with values determined by Kraft et al. (1996). Fe XANES spectra were also corrected for detector dead time.

For both the experimental glasses and J27 downflow samples described above, three individual V and Fe XANES spectra were collected to evaluate spectral heterogeneity. This confirmed that the variability in V and Fe XANES generally appeared to be ≤ 5% for the points chosen, as measured by the variation in intensity of the V and Fe pre-edge peaks between spectra. These multiple scans were summed to improve data quality for analysis. The same level of homogeneity was observed for the other natural samples analyzed, allowing summing of spectra to improve data quality. The exception to this was the pillow basalt sample from the East Pacific Rise, where the goal was to specifically evaluate in detail spatial heterogeneity in V and Fe speciation approaching the pillow rim.

The V and Fe XANES data were pre-processed using the ATHENA software package (Ravel and Newville 2005). In ATHENA, the below-edge normalization range was then set to -115.0 to -25.0 eV relative to an E_0 value 5480.00 eV and the above-edge normalization range was set to 110.0 to 132.0 eV. This ensures that the above-edge normalization is comparable to what was used in Sutton et al. (2005), i.e. 5600 eV. The normalized spectra (not flattened) were then exported from ATHENA to ASCII text files for MVA processing. The final, processed V K-edge XANES spectra for the experimental glasses are shown in Fig. 1 and for the unknown glasses in Fig. 2.

Given that Fe concentrations in the Hanson and Jones suite of glasses were not previously measured and significantly lower than those found in the natural basaltic starting materials, Fe abundance was estimated in this suite based on X-ray fluorescence compositional mapping (2 μm pixel size) using the 13-ID-E microprobe. Summed energy dispersive spectra were extracted from the maps based on compositional uniformity. Iron abundances were then calculated from the measured FeKα emission intensities using a standardless fundamental parameters algorithm (Criss et al. 1978), referenced to measured CaKα emission intensities and standardized to the Ca abundance reported by Hanson and Jones (1998). We estimate these calculated abundances have an uncertainty < 20%.

Multivariate Analysis Methods

The training of MVA models for the V XANES datasets presented here follows the general procedures described in Dyar et al. (2016a, 2016b) for Fe XANES analyses of silicate glasses and amphiboles. As was done in these studies for Fe, two multivariate techniques were tested: partial least-squares regression (PLS) and least absolute shrinkage and selection operator (Lasso). We find some key differences between these two techniques for V XANES.

PLS calculates which directions (vectors) maximize the covariance between two matrices of predicted and observable variables (Wegelin 2000). In the multivariate modeling presented here, these vectors define the model components, constructed from a matrix of intensity values at each of the 331 energy values in the XANES spectra (the observable variables) and the fO_2 relative to NNO buffer for each of the 28 experimental glasses analyzed (the predicted variables). PLS calculates a linear regression model by projecting both sets of variables to a new space, sequentially determining the model coefficients that maximize the covariance between the matrices. As discussed in the earlier work with Fe XANES (Dyar et al. 2016a, 2016b), for both

This is a preprint, the final version is subject to change, of the American Mineralogist (MSA)
Cite as Authors (Year) Title. American Mineralogist, in press.
DOI: https://doi.org/10.2138/am-2018-6319

PLS and Lasso, calculating the model coefficients is a two-step process. In the PLS case, first a shrinkage penalty is evaluated to determine the number of factors to be included in the regression. For V XANES, this reduces the number of channels at which the signal is measured as the number of components are varied. Once the optimal number of components (q) is determined, the second step follows ordinary least squares by regressing the response (here the fO_2 relative to NNO) to the components generated in the first step.

Lasso regression models (Tibshirani 1996) were also tested. Lasso assumes that a smaller subset of the predictor variables is driving the prediction results and thus produces a sparse model by shrinking some coefficients and setting most other coefficients to zero with no performance loss. Lasso also regularizes the least squares to prevent overfitting of the training data and includes a hyperparameter, α, that controls the constriction level of the coefficient vector. Lasso thus reduces a sizable, largely uninterpretable model to a sparse, more interpretable model.

For both the PLS and Lasso models explored here, MVA models were trained from the XANES results using the open-source machine learning Python library Scikit-learn (Pedregosa et al. 2011) and the Superman website at http://nemo.cs.umass.edu:54321 (Carey et al. 2017).

RESULTS AND DISCUSSION

Vanadium K-edge XANES Spectroscopy in Basaltic Glasses

Vanadium K edge XANES spectra for the 28 experimental glasses are shown in Fig. 1, color-coded as a function of their known, NNO-relative, oxygen fugacities at equilibration. The measured spectral intensities as a function of energy for these 28 glasses vary systematically with fO_2. In particular, distinct and systematic changes are observed in the structure and energy of the pre-edge feature, the absorption edge, and in the post-edge structure. Previous studies (Wong et

al. 1984) have evaluated in detail how measured V K-edge absorption features in XANES spectra relate to specific electronic transitions, metal valence state(s), and site geometry and symmetry. Much of that work is based on studies of V-bearing mineral compounds where the structural configuration of V within the mineral lattice is already fairly well understood. The variability in coordination geometry of the differing V species present in silicate melts and glasses is, by contrast, poorly characterized. Whereas the spectroscopic features observed for silicate glasses are comparable to those measured in V oxide minerals, the structures in the rising edge and white line are broader due to decreased ordering. To better evaluate the calibrations generated by our MVA models and understand how the energy channels chosen by our sparse models (the observable variables) relate to specific electronic and structure parameters in the experimental glasses, it is worth reviewing current thinking on the transitions and interactions that give rise to the major features observed within the spectra analyzed (these features are annotated on Fig. 1).

Vanadium measured by XANES in terrestrial basaltic glasses (~ 200-300 ppm) is almost exclusively bound to O^{2-} as the ligand, with a formal oxidation state that varies between V^{3+} to V^{5+}. In V oxide mineral phases, the coordination of V^{3+} is likely to be octahedral, whereas for V^{4+} and V^{5+} phases, distorted octahedral, tetrahedral, and square pyramidal geometries are possible (Wong et al. 1984; Keppler 1992) as enabled by the smaller size of the cations. In basaltic glasses, all of these oxidation states and coordination environments are possible and depend on features of the V-O bonding discussed here and the overall glass structure discussed below for different glass compositions.

The pre-edge feature observed in the experimental glass spectra (Fig. 1) results from the dipole forbidden l*s*→3*d* transition, which is allowed primarily due to mixing and overlap with

the 2*p* orbitals of the oxygen ligand. With increasing valence state, nuclear shielding of the core electrons decreases, resulting in a shift of the pre-edge to higher energy. The pre-edge peak intensity is coupled to the metal-ligand symmetry; V species in regular octahedral coordination with the O^{2-} ligand have the smallest observable pre-edge intensity while species in tetrahedral coordination have the largest intensity. The pre-edge also displays a varying multiplet structure caused by crystal-field splitting of the ground state. In the experimental glasses analyzed, all these pre-edge features vary systematically with increasing fO_2 at equilibration; systematic changes are observed in the pre-edge multiplet structure along with increases in the energy and intensity of the multiplet peaks.

The dipole-allowed 1*s*→4*p* transition gives rise to the observed V K-edge main edge and white line. A low energy shoulder on the rising absorption edge is often attributed to the 1*s*→4*p* shakedown transition. Valence bond configuration modeling suggests that differences in the energy and intensity of the rising edge transition and white line reflect variations in metal-ligand overlap and covalency. Absorption features above the white line can be attributed to several competing interactions including the transition to higher *np* states, shape resonances, and multiple scattering effects (Wong et al. 1984).

Wong et al. (1984) show that the energy positions of all these different absorption features in V oxide minerals, including pre-edge features, increase with increasing V oxidation state. However, the relative energy shift observed for each of these features as a function of larger formal valence differs due to binding of the inner 3*d* and 4*s* levels relative to the outer 4*p* levels. This is consistent with what is observed in the experimental glasses measured here as a function of fO_2. Also observed are systematic decreases in the relative intensity of the white line and first multiple scattering resonance with increasing fO_2. As described above, all these energy shifts

This is a preprint, the final version is subject to change, of the American Mineralogist (MSA)
Cite as Authors (Year) Title. American Mineralogist, in press.
DOI: https://doi.org/10.2138/am-2018-6319

arise from changes in V "chemical state": valence, electronegativity of the bonding ligands, coordination number, and other structural features. The systematic growth in intensity of the absorption features with energy position and fO_2 in the experimental glass spectra makes them ideally suited for MVA modeling as it allows development of non-linear predictive models that directly relate the fO_2 of the glasses at equilibration to the intensity response of those energy channels that contain the most highly-weighted information.

Multivariate Calibration Models for Experimental Glasses

Using the XANES analyses of the 28 experimental glasses, several permutations of multivariate calibration models were tested to relate the full measured spectral range to fO_2 (relative to NNO buffer). For both PLS and Lasso models generated, the ΔNNO value for a measured spectrum can then be calculated using the sum-of-products of the normalized spectral intensity (I_E) and corresponding calculated coefficient (C_E) at each of the energy channels as follows:

$$\Delta NNO = I_{E1}C_{E1} + I_{E2}C_{E2} + I_{E3}C_{E3} + \ldots \quad (1)$$

For modeling, the input spectra were truncated so that the energy range extended from 5400.0 – 5613.0 eV, regularized to an energy step of 0.1 eV and normalized to 5600.0 eV. Both PLS and Lasso models were evaluated using variable hyperparameter values. For PLS models, we evaluated q values between 2 and 8, whereas sparsity parameter values of α between 0.01 and 0.0001 were tested for Lasso. Predictor variables for the MVA models consist of the matrix of intensity values at each of the 331 energies in the XANES spectra for each of the 28 samples analyzed.

For the PLS models, a single response model, PLS-1, was trained for prediction of our variable of interest, which was the value of log fO_2 relative to NNO buffer. For the full-spectrum

models, the first local minimum value of the root-mean-square-error (RMSE) in component space occurred at a value of $q = 4$. This model results in a leave-one-out cross-validated RMSE (LOO-RMSE-CV) of 0.75 and an internal cross-validated RMSE of 0.53 (Fig. 3). Leave-one-out cross-validation generally produces the best estimate of prediction error on unseen data when the training population is high. We have chosen to report the internally validated RMSE in the figures and tables because, for models trained on relatively small populations (as is the case here with n=28), LOO-RMSE-CV tends to give a more biased estimation of the expected loss on the population, whereas the internal RMSE incorporates the statistics of the estimator on the full data-set. We conclude that PLS models with $q = 4$ provide the most accurate predictions for fO_2 when using these 28 experimental input spectra with RMSE of 0.53. For PLS models, the q value does not relate directly to the predicted variable, but is instead comparable to the order of a polynomial used to fit the data (Dyar et al. 2016b). Low values (of q) indicate generalizable models useful for unseen data, while higher values may produce overfitting. A plot of calculated PLS coefficients as a function of the energy channels with a q value of 4 (Fig. 3) shows that the channels that are most highly correlated with predicted fO_2 (with the largest positive and negative values) are those in the pre-edge, main-edge, and white line.

The relative performance of the Lasso models for the V XANES oxybarometer appears to be generally better than the PLS models with the added advantage that the Lasso models are sparse and more generalizable. Figures 4 and 5 summarize the results of three different Lasso models where α was set to 0.01, 0.001 and 0.0001. At these three hyperparameter values, the respective internal model RMSE's returned were 0.70 ($R^2 = 0.95$), 0.36 ($R^2 = 0.99$) and 0.08 ($R^2 = 1.00$) respectively. However, at α values lower than 0.0008, the Lasso model abruptly begins to overfit the model to the data so that spectral noise begins to be inappropriately weighted. This is clear in

Fig. 4 (α = 0.0001) where channels below the pre-edge peak energy (< 5460 eV) and near the normalization energy in the edge step (~ 5590 eV) begin to be highly correlated to the predicted variable. However, because there are only a handful of nonzero coefficients in the Lasso model, overfitting is generally less of a concern. It thus seems that the best choice for Lasso model parameters for this data set (using these 28 experimental training glasses) is α = 0.0008 (internal RMSE = 0.33, R^2 = 0.99), though it is quite similar to the results provided by the α = 0.001 model (internal RMSE = 0.36, R^2 = 0.99). The LOO-RMSE-CV of the α = 0.0008 model is 0.87, but again we report the internal RMSE on the figures and tables as this is likely less biased given the small population size. The calculated uncertainty of this model for the predicted variable is thus comparable to the assumed experimental uncertainty in estimating log fO_2 in the experimental glasses (~ 0.1–0.2 log units). However, this model is still fairly sparse; only 12 channels in the V XANES spectra are used to predict the log fO_2 relative to NNO buffer (not the 331 required by the PLS modeling). The channels chosen by the model all correspond to significant spectral features (Fig. 4, α = 0.001); these are five energy channels in the pre-edge peak, five channels in the rising absorption edge and on the white line, and two channels on the multiple scattering resonance immediately following the white line.

The ΔNNO value for a measured spectrum (normalized as described above) can then be calculated for this α = 0.0008 Lasso model, using Equation 1, at each of the 12 energy channels (Table 6). Reducing the number of channels needed for fO_2 prediction to such a small number is crucial for rapidly generating high-resolution redox maps with ~1 μm pixel resolution by mapping the fluorescence intensity at these 12 energies and using the Lasso coefficients to convert the mapped intensities directly to NNO relative fO_2.

Uncertainties due to Temperature Dependence of Redox Buffer and V Valence

This is a preprint, the final version is subject to change, of the American Mineralogist (MSA)
Cite as Authors (Year) Title. American Mineralogist, in press.
DOI: https://doi.org/10.2138/am-2018-6319

Valence states of the V redox couples have a dependence on both fO_2 and temperature. With decreasing temperature, V becomes more oxidized. This follows a Clausius-Clapeyron relationship such that the log of the redox couple ratio is linear in 1/T and proportional to the redox reaction enthalpy. The V XANES oxybarometer presented in Sutton et al. (2005), which calibrates the V pre-edge peak intensity to fO_2, thus required temperature corrections for the standards because they were synthesized at different temperatures.

The Ni-NiO oxygen buffer, against which the MVA oxybarometer model presented here is calibrated, also has a well-defined temperature-oxygen fugacity (T-fO_2) relationship (Huebner and Sato 1970; O'Neill and Pownceby 1993). If the T-fO_2 relationship of the NNO buffer and V redox couple are approximately parallel, then a calibration relating the measured XANES to the buffer relative fO_2 of a glass at the time of equilibration has the advantage of not requiring a priori knowledge of the glass's equilibration temperature. This parallelism of T-fO_2 is likely if the reaction enthalpy of the buffer generally parallels the reduction enthalpies for the V redox couples (e.g., Schreiber 1986), particularly over the typical range of equilibration temperatures for basaltic melts (~ 980°C - 1280°C). However, if the T-fO_2 curves are not parallel, then the model will include a temperature dependent uncertainty that may be significant.

The T-fO_2 relationship for the NNO buffer is well constrained from previous studies (Huebner and Sato 1970; O'Neill and Pownceby 1993). Based on the work of O'Neill and Pownceby (1993), over the temperature range of 700-1700K, the NNO T-fO_2 relationship can be approximated by:

$$\log fO_2 = 12.9792 - \frac{25015.1}{T\ (K)} - 0.51162 * \ln(T\ (K)) + 0.046 * \frac{P\ (bars) - 1}{T\ (K)} \qquad (2)$$

However, the T-fO_2 relationship for the various V redox couples in silicate glasses is not well constrained experimentally. Johnston (1965) conducted a series of experiments examining the

valence state behavior of V in sodium disilicate ($Na_2O{\cdot}2SiO_2$) melts. Based on this data, Borisov (2013) proposed the following relationships to relate the proportions of the redox states of V to T-fO_2:

$$\log fO_2 = \left(\log\left(\frac{X_{V^{5+}}}{X_{V^{4+}}}\right) - \frac{4154.4}{T\,(K)} + 0.32\right) * 4 \quad (3)$$

$$\log fO_2 = \left(\log\left(\frac{X_{V^{4+}}}{X_{V^{3+}}}\right) - \frac{6149.0}{T\,(K)} + 0.77\right) * 4 \quad (4)$$

$$\log fO_2 = \left(\log\left(\frac{X_{V^{3+}}}{X_{V^{2+}}}\right) - \frac{7929.9}{T\,(K)} - 0.12\right) * 4 \quad (5)$$

Following the approach proposed by Borisov (2013), we compared the equations for the V redox pairs (equations 3 to 5) with the T-fO_2 relationship of the NNO buffer (NNO 0; equation 2). This is shown in Fig. 6, calculated between 980°C-1280°C, the range of temperatures most relevant for terrestrial basaltic glasses. The starting point for the V calculations is T = 1553K, fO_2 = -6.68, with the corresponding changes in the intrinsic oxygen fugacity of melt evaluated for a cooling melt under closed system conditions. For terrestrial basalts, the V^{4+}/V^{3+} couple dominates. While V^{2+} may potentially be present in highly reduced, extraterrestrial glasses, it has never been identified in terrestrial basalts. The V^{5+}/V^{4+} redox couple will begin to be important in more oxidized systems, but published XANES data for terrestrial basaltic glasses generally show that their V* typically lies between V^{3+} and V^{4+} (Canil 1997; Sutton et al. 2005; Karner et al. 2006). The calculated V valence relationships in Fig. 6 show that the T-fO_2 trend of the V^{4+}/V^{3+} couple is almost identical to the slope of the NNO buffer. At 980°C, the maximum thermal extent calculated here relative to a starting T of 1280°C, the calculated difference in log fO_2 between the NNO buffer and the V^{4+}/V^{3+} couple is < 0.05. Thus, if it is reasonable to assume that the V^{4+}/V^{3+} redox couple is the dominant control on V valence for terrestrial basaltic melts, the temperature uncertainty introduced by calibrating the MVA model relative to NNO is likely

negligible compared to the calculated RMSE of the model. In more oxidized melts, where the V^{5+}/V^{4+} redox couple becomes more prevalent, the relative uncertainty of the model will likely increase if the calibration model retains a reference to NNO. For these melts, a model referenced to a different buffer may be more appropriate. Of course, these estimates are based on experiments carried out with $Na_2O{\cdot}2SiO_2$ melts and there may be compositional differences with respect to basaltic melts. Experiments that explore compositions relevant to natural glasses with respect to V valence would be particularly useful to resolve this issue.

Relative fO_2 Dependence of V Speciation in High- vs Low-Fe Glasses

The MVA models evaluated here are constructed using 28 synthetic glasses. Of these, 22 were synthesized from natural basaltic starting materials with FeO_T contents that range from 6.9 – 12.7 wt% (mean = 10.4 wt%, $1\sigma \pm 1.5$), so that Fe/V >>1. The remaining six are from the Hanson and Jones suite of glasses, synthesized from reagent grade oxide powders to generate glasses of FAD composition with a V dopant and, based on our XANES analysis, also containing trace levels of Fe (Fe/V $\lesssim$1). Estimated Fe abundances vary from ~ 47 to 8600 ppm (Table 7), significantly lower than that of typical terrestrial basaltic melts (~ 10 wt% FeO_T). It is possible that the V XANES oxybarometric models have a compositional dependence on the melt Fe/V ratio that results in systematic differences between the V valence of the glass relative to that of the respective melt (Borisov 2013). It is also likely that the average coordination of the available oxygens will have a compositional dependence. The observed variation in Fe content in the synthetic glasses analyzed provides an opportunity to evaluate possible interactions between V^{4+}-V^{5+} and V^{3+}-V^{4+} redox pairs relative to the Fe^{2+}- Fe^{3+} redox pair at equilibration.

In the FAD experimental suite, both V and Fe show systematic increases in valence as a function of the measured fO_2 at equilibration conditions (Fig. 7), as would be expected. The

observed differences in V spectra as a function of fO_2 are consistent with those measured in glasses synthesized from natural basaltic starting materials. This is demonstrated in Fig. 7 (left panels) where V XANES spectra from FAD and natural basaltic glasses that are reported to have been equilibrated at similar nominal fO_2's (~ NNO-3.3, NNO-0.7, NNO+1.8) are compared. Although there are small differences that may reflect uncertainties in the fO_2 at equilibration, overall there is good agreement between the measured vanadium spectroscopic features (pre-edge peak energy positions and intensities, structure and energy position of the rising edge, white line energy position and intensity, and post edge structure) at all oxygen fugacities. On the other hand, Fe XANES spectra (Fig. 7, right panels) clearly indicate that Fe has a higher valence state in the FAD glasses compared to glasses synthesized from natural basaltic materials at a given fO_2. There are large differences in the Fe pre-edge multiplet structure, in E_0 and in the white line energy consistent with increased effective Fe valence (King et al. 2000; Galoisy et al. 2001; Berry et al. 2003; Wilke et al. 2005; Cottrell et al. 2009; Dyar et al. 2016a). The systematic difference between fO_2 predicted by V and Fe XANES for these glasses doesn't seem to be correlated with Fe/V, nor does it seem to depend on fO_2.

Considering that the Fe content of the synthesized FAD glasses was not controlled during their synthesis, more careful experimental studies are required to determine the impact on the V XANES due to varying Fe/V ratio. It is not surprising that the effective Fe valence shows an offset in fO_2 between the Mg-rich FAD compositions, where Fe is a trace element, and the natural basaltic compositions, where Fe is a major element. It has been well established that at major element concentrations, the coordination state of Fe in silicate melts is sensitive to the liquid composition (Dickenson and Hess 1982, 1986; Kress and Carmichael 1991; Schreiber et al. 1994). The exact mechanism that leads the Fe to be more oxidized than predicted is not yet

clear. For Cr doped glasses, Hanson and Jones (1998) hypothesized that the presence of Fe^{3+} in their iron-bearing systems suppressed the formation of Cr^{2+}, moving the transition fO_2 of the redox pair to lower values and resulting in Cr valences that appear more oxidized than predicted. In the case of these V doped glasses, where Fe abundances are similar or significantly lower that the V abundance, it may be possible that V^{4+} and V^{5+}, which increase proportionally relative to V^{3+} with increasing fO_2, may similarly be causing the suppression of Fe^{2+}.

This observation aside, the most important result with respect to the MVA modeling is that at trace V concentrations (3000 ppm and lower), Fe appears to have no measurable oxidizing effect on V valence. The influence of Fe/V ratio on V speciation at equilibration appears to be negligible, with melt fO_2 exerting the primary control on the discrete V valence states that will exist in quenched glasses. Sutton et al. (2005) showed that the V pre-edge peak intensity shows a slight composition dependence when comparing spectra measured in high Ca FAD glasses to low Ca forsterite-anorthite-silica (FAS) glasses equilibrated at the nominally similar fO_2. They estimated that the structural effect on V pre-edge intensity for basaltic glasses would results in at most a maximum potential oxygen fugacity error of ~0.5 log units in fO_2. This is consistent with the observation made here in comparing FAD and basaltic compositions, which shows that impacts on calculated NNO-relative fO_2 appear to be within the calculated uncertainties of the model. This increases confidence in the MVA models presented here, particularly over the compositional range represented by basaltic melts.

Modeling fO_2 of Natural Basaltic Glasses

Microprobe Standard Glasses

The Lasso calibration model was applied to V XANES spectra measured on three basaltic glass samples available from the USGS (BCR-2G) and the Smithsonian Institution (A-99 and

VG-2) for use as electron microprobe standards. Their measured V spectra are shown in Fig. 2 and the predicted oxygen fugacities from the model are shown in Table 3. Note that the 1σ uncertainties in predicted fO_2 relative to NNO using the Lasso model with $\alpha = 0.0008$ are ±0.33 log units.

Applying the Lasso model to data from glass standard BCR-2G gives fO_2 of NNO+1.08. There are no experimental data that constrain the oxygen fugacity at equilibration for this glass, although the temperature (1540 °C) and atmospheric composition (nitrogen gas) at quench are known (Wilson and Taggart 2000).

The NMNH standard A-99 consists of samples of fresh basaltic glass collected from the Makaopuhi lava lake, Hawaii in 1965 (Wright and Okamura 1977) and provides a calculated fO_2 of NNO-1.28. This is slightly lower than fO_2 values measured using oxygen sensors inserted within drill holes in the lake (Sato and Wright 1966; Wright and Okamura 1977), but within the estimated uncertainty. Oxygen fugacities measured using these sensors at Makaopuhi were generally within one log unit of the NNO reference buffer (Wright and Okamura 1977), although fO_2 was found to increase as the lake cooled and it is unclear exactly when and where sample A-99 was collected. However, values of fO_2 for Makaopuhi lake samples based on Fe^{3+}/Fe^{2+} ratios measured by wet chemistry (Sack et al. 1980) are about 0.4 log fO_2 units lower than those measured using oxygen sensors during collection (when calculated at T > 1100°C), so still within estimated uncertainty of our Lasso model. The Lasso model value for fO_2 from V XANES is also consistent with fO_2 values calculated from iron redox geobarometry of glassy, subaerial Kilauea lavas by Carmichael and Ghiorso (1990), which give an average of NNO-1.08.

NMNH VG-2 consists of samples of fresh basaltic glass dredged from the median valley of the Juan de Fuca Ridge (Jarosewich et al. 1980; Jarosewich 2002). Our V XANES oxybarometer

calibration gives fO_2 of NNO-0.08 for this sample. On the basis of Fe valence calculated by the Fe XANES pre-edge centroid method, Cottrell and Kelley (2011) quote a calculated fO_2 for standard VG-2 of QFM+0.26, or NNO-0.47. Our value for fO_2 from V XANES is slightly more oxidized than what has previously been calculated using Fe XANES outside the predicted uncertainty of the MVA model (± 0.33 1σ).

Kilauea Downflow Sequence

Natural basaltic glasses from an active lava flow at Kilauea were also analyzed, with samples collected at various distances from the primary vent between 3.4 and 18.7 km downflow (HVO sequence J27, Table 4). The motivation for this study was to evaluate if the V XANES and MVA method generated are able to see variability in fO_2 over flow distance. Processes such as pre/syn-eruptive sulfur degassing, for example, may lead to changes in observed fO_2 (Anderson and Wright 1972). Each sample in this suite consisted of several glass fragments mounted in epoxy. The samples contain ~75-90% glass with small amounts of crystalline material primarily in the form of pyroxene and plagioclase. SEM (Fig. 8) images and μXRF analyses of the samples prior to XANES studies were used to avoid the contribution of any such crystalline material in measured spectra. For each of the seven samples, three separate V and Fe XANES spectra were collected, each on a different fragment of glass. Less than 5% difference was observed in normalized spectral intensities between the three analyses for each of the samples examined and thus the spectra were considered to represent glass and summed. The summed spectra are shown in Fig. 8 for both V and Fe, color-coded with respect to the sampling distance from the vent in kilometers. Values for predicted NNO-relative fO_2 from the Lasso model with $\alpha = 0.0008$ and values for predicted $Fe^{3+}/\Sigma Fe$, using the Dyar et al. (2016a) calibration, are shown in Table 4. The Dyar et al. (2016a) Fe calibration quotes a LOO- RMSE-CV error on prediction of $\%Fe^{3+}$ in

glasses of ±3.6 %Fe^{3+}. Also shown are values for predicted NNO-relative fO_2 calculated using the Kress and Carmichael (1991) Fe-redox equilibrium equation based on the predicted $Fe^{3+}/\Sigma Fe$ and measured glass composition. The mean fO_2 for the seven samples based on the V oxybarometry is NNO-1.15 ±0.19 (1σ) and based on the Fe oxybarometry is NNO-1.08 ±0.20 (1σ), with inter-sample variability being smaller than the RMSE from the model. While the $Fe^{3+}/\Sigma Fe$ ratios for the individual samples suggest a very small overall increase of 0.03 with distance, careful examination of the measured spectra (Fig. 8) shows no convincing differences in Fe speciation between the seven samples analyzed. For these samples, the V and Fe XANES oxybarometry provide consistent and precise estimates for fO_2 well within uncertainty, and indicates no significant change in melt oxidation state with distance downflow. The fO_2 of these samples from the V XANES oxybarometry, NNO-1.15 (±0.19 1σ of the mean), is also consistent with that measured for microprobe standard A-99 collected at Makaopuhi lava lake, NNO-1.28 (±0.33 model RMSE). As described earlier, it is also consistent with the average fO_2 of NNO-1.08 found for subaerial Kilauea lavas by Carmichael and Ghiorso (1990).

East Pacific Rise MORB Pillow Basalt

Microfocused V and Fe XANES spectra were measured from a sample of pillow basalt glass dredged from the East Pacific Rise (EPR). The glassy zone where the measurements were taken consists of light brown isotropic glass with scattered microlites (Fig. 9 left), consistent with the petrographic features described in other Pacific Ocean pillow basalts (Baragar et al. 1977; Marescotti et al. 2000). Nine individual V and Fe XANES spectra were collected in glass extending ~5.5 mm into the pillow from its quenched surface. To minimize the potential contribution of microlites to the measured XANES spectra, the analytical points were chosen on the basis of XRF compositional mapping. Fig. 9 (left) displays the FeKα compositional map

with the selected analysis points indicated as an overlay on the plane light photomicrograph of the pillow rim. A focused 2x2 μm X-ray beam was used to collect the spectra with the V and Fe analysis points offset vertically by ~20 μm from one another (at a given distance in to the rim) to ensure that fresh glass was being analyzed in each case. The motivation for this part of the study was to evaluate if gradients in oxidation are recognizable within the glassy rim from either V or Fe XANES.

The V and Fe XANES spectra are shown in Fig. 9 (right panels), color-coded with respect to the sampling distance from the pillow surface in millimeters. The precise distances from the rim are shown in Table 5, along with values of NNO-relative fO_2 from the Lasso model with α = 0.0008, predicted $Fe^{3+}/\Sigma Fe$ (using the Dyar et al. 2016a calibration), NNO-relative fO_2 from the predicted $Fe^{3+}/\Sigma Fe$ and glass composition, and the measured Fe XANES pre-edge peak centroid energy for each spectra. The fO_2 determined for the nine analysis points from V oxybarometry varies from NNO-2.67 (±0.33) to NNO-3.72 (±0.33) with distance from the rim. The mean fO_2 from V XANES oxybarometry is NNO-2.62. The mean $Fe^{3+}/\Sigma Fe$ from the Fe XANES is 0.074, which is consistent with an fO_2 of NNO-2.54 for the given glass composition and very close to the mean fO_2 from V XANES. The calculated fO_2 values from V and Fe XANES from this sample are both slightly more reduced than estimates of the average fO_2 for MORB, where published mean values range between ~NNO-2.0 and ~NNO-0.6 (Christie et al. 1986; Bézos and Humler 2005; Cottrell and Kelley 2011). Samples of EPR glasses from this vicinity are reported by Christie et al. (1986) to have fO_2 as low as NNO-3.02. The relatively low measured $Fe^{3+}/\Sigma Fe$ in this sample provides an opportunity to more carefully evaluate relative differences in predicted fO_2 based on both V and Fe XANES in a basaltic glass where $Fe^{3+}/\Sigma Fe$ ratios appear to be < 0.1.

As described above, the $Fe^{3+}/\Sigma Fe$ ratios for the nine individual analysis points are similar to each other within the stated ±3.6 $\%Fe^{3+}$ uncertainty of the Fe XANES MVA model (Dyar et al. 2016a). The measured Fe XANES spectra for these nine points show no evidence for changes in Fe valence state with distance. This is most easily evaluated by comparing the Fe XANES pre-edge peak centroid energies for the nine analysis points, which give a mean value of 7111.93 ±0.01 (1σ) eV and are indistinguishable from each other within analytical uncertainty. A similar experiment by Cottrell and Kelley (2011) looking at Fe XANES spectra collected through a MORB pillow from the Carlsberg Ridge came to the same conclusion, that sampling of locations through ~ 16 mm of pillow glass recorded the same Fe XANES centroid position within error.

However, the calculated fO_2's based on V oxybarometry lie outside the ±0.33 RMSE of the Lasso model. Close inspection of the V XANES spectra (Fig. 9, top right) shows systematic variation in the intensity of the absorption features, with the pre-edge peak intensity decreasing, the edge position shifting to lower energy, and the white line intensity increasing with distance from the rim, consistent with more reduced V away from the rim. Thus, a systematic oxidation in V is observed outward towards the pillow rim over this ~ 5 mm distance at the analytical precision of the XANES analysis, corresponding to a decrease in fO_2 of ~ 1 log unit.

The discrepancy between the results from V and Fe XANES is potentially significant. This may imply that there are processes that impact V and Fe speciation differently through the glassy portion of the pillow rim. However, a more likely explanation is that Fe XANES in basaltic glasses seems to be insensitive to changes in fO_2 below a certain threshold, which is higher for Fe than for V. We hypothesize that at these reduced compositions, $Fe^{3+}/\Sigma Fe$ ratios < 0.1, changes in fO_2 of ~ 1 log unit are difficult to detect in basaltic glasses using Fe K-edge XANES. It can be predicted (Kress and Carmichael 1991) that in these glasses a 1 log unit reduction in fO_2 from

NNO-2.7 to NNO-3.7 would result in a decrease in $Fe^{3+}/\Sigma Fe$ of only ~ 2.5%. Fe XANES fO_2 calibration curves presented by Cottrell et al. (2009) demonstrate that at the reduced end member compositions, a 10% change in $Fe^{3+}/\Sigma Fe$ would appear to lead to about an ~ 0.3 eV change in the pre-edge peak centroid position. This appears to be consistent with the measurements presented here and illustrates that for reduced basaltic glasses, V XANES oxybarometry is likely to be more sensitive to changes in fO_2.

IMPLICATIONS

This research demonstrates how MVA modeling of V XANES, using the full XANES spectrum, can be used to determine the oxygen fugacity at which basaltic silicate glasses equilibrated. Our previous studies on Fe XANES spectra measured in glasses and amphiboles (Dyar et al. 2016b, 2016a) demonstrated that MVA using the full Fe XANES spectrum can independently identify which spectroscopic components are the most strongly correlated to the predicted variable of interest, such as the average Fe valence.

We expand this concept and highlight the potential for using MVA XANES modeling to relate the measured spectral features directly to oxygen fugacity as the predicted variable. Calibrating to buffer-relative fO_2 greatly expands the potential suite of experimental glasses that can be used to train the model, since an independent measure of the glass's V valence is not required. However, this approach does assume that the V redox equilibria in basaltic silicate melts, and thus speciation as measured by XANES, is controlled primarily by oxygen fugacity. While this is largely true, other intensive properties of the system, particularly equilibration temperature and chemical composition, will have an impact on the V redox equilibria. Thus the approach requires that uncertainties introduced by variability in equilibration temperature and melt composition be small relative to the calculated model uncertainty.

Restricting the calibration model to glasses of basaltic composition decreases the potential uncertainties due to variations in melt composition, the most significant of which is likely to be variability in the Fe/V ratio of the melt. Comparison of V XANES spectra collected in glasses synthesized from natural basaltic compositions, where Fe/V ratios are generally > 250, and for glasses synthesized from FAD compositions, where Fe/V ratios are generally $\lesssim 1$, shows that the XANES are comparable for glasses equilibrated at similar fO_2, even though there are large differences in major element composition. Therefore, at least for glasses that cover the typical range of basaltic compositions that might be modeled, uncertainties introduced due to expected compositional variations are likely small.

Similarly, some researchers have questioned whether valence state ratios for trace elements are quenchable in Fe-bearing systems (Berry et al. 2006; Borisov 2013). This is because rapid electron transfer from Fe^{2+} may have the potential to reduce a minor, oxidized species during a relatively slow quench that might last for several seconds. The driving thermodynamic force behind this issue is that the V^{3+}/V^{4+} buffer does not perfectly parallel that of the Fe^{2+}/Fe^{3+} buffer as temperature changes. Therefore, it is argued that at least some electron transfer should be expected. In Fe-free systems these effects are likely small because the species of interest, V^{3+}, V^{4+}, and V^{5+}, are dilute to the extent that they may not electronically communicate, even on the timescale of seconds. Yet even here, the observation that the V XANES are comparable for nominally Fe-free FAD and Fe-bearing natural basaltic glasses equilibrated at similar fO_2 suggests that changes in V valence that may result from electron transfer are likely small within the calculated uncertainties of the calibration models.

Uncertainties that may arise due to variations in equilibration temperature are important to evaluate because the valence states of redox couples are known to be dependent on temperature.

A key assumption in this study is that such T-relative uncertainties can be minimized by calibrating the MVA model directly against NNO-relative fO_2. This is most likely valid if the reaction enthalpy of the buffer the model is calibrated against generally parallels the reduction enthalpies for the V redox couples. The modeling here suggests this is a reasonable assumption, with the T-fO_2 trend of the V^{4+}/V^{3+} couple having nearly identical slope as the NNO buffer. Future V XANES studies that use experimental glasses synthesized at not only variable fO_2, but quenched at varying T and over a range of compositions will more precisely constrain the impact of these variables on the V speciation and lead to improvements in model precision and accuracy.

Applied to natural glasses of basaltic composition, this V XANES oxybarometer provides an additional constraint on the fO_2 conditions at which the melts equilibrated. Overall, the V XANES oxybarometry model presented here yields predicted NNO-relative fO_2 values that are within analytical uncertainty of what is calculated using Fe XANES to predict $Fe^{3+}/\Sigma Fe$. For the two suites of analyses presented here from a basaltic lava flow at Kilauea and from MORB-type pillow basalt glass from the East Pacific Rise, the average of the fO_2 estimates provided by V and Fe XANES oxybarometry show close agreement, further validating the modeling approach. For the Kilauea downflow sequence, the mean fO_2 based on V oxybarometry is NNO-1.15 and based on Fe oxybarometry it is NNO-1.08 ±0.20, essentially indistinguishable within inter-sample variability.

The same is generally true for the sequence of analyses from the more reduced East Pacific Rise pillow glass. The mean calculated fO_2 based on the V XANES oxybarometry of nine individual points in the sample is NNO-2.62, and based on Fe XANES oxybarometry the mean calculated fO_2 is NNO-2.54. However, in detail it is clear that systematic, measurable changes

This is a preprint, the final version is subject to change, of the American Mineralogist (MSA)
Cite as Authors (Year) Title. American Mineralogist, in press.
DOI: https://doi.org/10.2138/am-2018-6319

are observed in V XANES over the length of pillow rim analyzed, while there is no perceptible, measurable difference in the Fe XANES. It is possible that these differences potentially reflect variations in the geochemical behavior of V in comparison to Fe with respect to changes in melt composition, oxidation, or cooling rate at the pillow margin as the melt quenches and the glass alters. There may, for example, potentially be differences in the buffering of Fe as compared to V if there are changes in bulk chemistry (Dickenson and Hess 1986) within the rim margin.

However, it seems more likely that for reduced, basaltic glasses with $Fe^{3+}/\Sigma Fe$ ratios below ~0.1, V XANES oxybarometry appears to have greater sensitivity to small changes in fO_2 than can be detected using Fe XANES. The data presented in this study are consistent with the observation that Fe XANES may be less sensitive in detecting continued decreases in the Fe^{3+} content for basaltic glasses equilibrated at conditions more reduced than ~ NNO-2. These are conditions particularly relevant not only in studying MORB, but also in evaluating the petrogenesis of highly reduced glasses from the Moon, Mars or meteorites.

ACKNOWLEDGEMENTS

This research was supported by the Remote, In Situ, and Synchrotron Studies for Science and Exploration (RIS^{4}E) node of the NASA SSERVI program and NASA grants NNX16AR18G and NNX17AL07G. XANES spectroscopy data were collected at GeoSoilEnviroCARS (Sector 13), Advanced Photon Source (APS), Argonne National Laboratory. GeoSoilEnviroCARS is supported by the National Science Foundation, Earth Sciences (EAR-1128799) and Department of Energy, Geosciences (DE-FG02-94ER14466). Use of the Advanced Photon Source was supported by the U.S. Department of Energy, Office of Science, Office of Basic Energy Sciences, under contract no. DE-AC02-06CH11357. King was supported by an Australian Research Council Future Fellowship (FT130101524).

We acknowledge the Smithsonian Institute National Museum of Natural History Department of Mineral Sciences for the use of NMNH 117393 basalt reference glasses for this study and for providing samples of basaltic glass standards VG-2 (NMNH 111240-52) and A-99 (NMNH 113498-1). We wish to thank Joe Boesenberg (Brown University) for tremendous help with sample preparation and electron probe data collection. We also wish to thank Anne Gardulski for providing us with the EPR pillow basalt sample.

REFERENCES CITED

Anderson, A.T., and Wright, T.L. (1972) Phenocrysts and glass inclusions and their bearing on oxidation and mixing of basaltic magmas, Kilauea volcano, Hawaii. American Mineralogist, 57, 188.

Ballhaus, C., Berry, R.F., and Green, D.H. (1990) Oxygen fugacity controls in the Earth's upper mantle. Nature, 348, 437–440.

Baragar, W.R.A., Plant, A.G., Pringle, G.J., and Schau, M. (1977) Petrology and alteration of selected units of Mid-Atlantic Ridge basalts sampled from sites 332 and 335, DSDP. Canadian Journal of Earth Sciences, 14, 837–874.

Berry, A.J., O'Neill, H.S.C., Jayasuriya, K.D., Campbell, S.J., and Foran, G.J. (2003) XANES calibrations for the oxidation state of iron in a silicate glass. American Mineralogist, 88, 967–977.

Berry, A.J., O'Neill, H.S.C., Scott, D.R., Foran, G.J., and Shelley, J.M.G. (2006) The effect of composition on Cr^{2+}/Cr^{3+} in silicate melts. American Mineralogist, 91, 1901–1908.

Bézos, A., and Humler, E. (2005) The $Fe^{3+}/\Sigma Fe$ ratios of MORB glasses and their implications for mantle melting. Geochimica et Cosmochimica Acta, 69, 711–725.

Borisov, A.A. (2013) Mutual interaction of redox pairs in silicate melts: $V^{5+}/V^{4+}/V^{3+}/V^{2+}$ tetrad and other equilibria. Petrology, 21, 305–315.

Canil, D. (1997) Vanadium partitioning and the oxidation state of Archaean komatiite magmas. Nature, 389, 842–845.

——— (1999) Vanadium partitioning between orthopyroxene, spinel and silicate melt and the redox states of mantle source regions for primary magmas. Geochimica et Cosmochimica Acta, 63, 557–572.

Canil, D., and Fedortchouk, Y. (2001) Olivine–liquid partitioning of vanadium and other trace elements, with applications to modern and ancient picrites. The Canadian Mineralogist, 39, 319–330.

Carey, C., Dyar, M.D., Boucher, T., and Giguere, S. (2017) Web-Based Software for Preprocessing, Matching, Fitting, Prediction, and Visualization of Spectroscopic Data: The Data Exploration, Visualization, and Analysis of Spectra (DEVAS) Website. In Lunar and Planetary Science Conference Vol. 48.

Carmichael, I.S., and Ghiorso, M.S. (1990) The effect of oxygen fugacity on the redox state of natural liquids and their crystallizing phases. Reviews in Mineralogy and Geochemistry, 24, 191–212.

Carmichael, I.S.E. (1991) The redox states of basic and silicic magmas: a reflection of their source regions? Contributions to Mineralogy and Petrology, 106, 129–141.

Christie, D.M., Carmichael, I.S., and Langmuir, C.H. (1986) Oxidation states of mid-ocean ridge basalt glasses. Earth and Planetary Science Letters, 79, 397–411.

Cottrell, E., and Kelley, K.A. (2011) The oxidation state of Fe in MORB glasses and the oxygen fugacity of the upper mantle. Earth and Planetary Science Letters, 305, 270–282.

Cottrell, E., Kelley, K.A., Lanzirotti, A., and Fischer, R.A. (2009) High-precision determination of iron oxidation state in silicate glasses using XANES. Chemical Geology, 268, 167–179.

Criss, J.W., Birks, L.S., and Gilfrich, J.V. (1978) Versatile x-ray analysis program combining fundamental parameters and empirical coefficients. Analytical Chemistry, 50, 33–37.

de Moor, J.M., Fischer, T.P., Sharp, Z.D., King, P.L., Wilke, M., Botcharnikov, R.E., Cottrell, E., Zelenski, M., Marty, B., and Klimm, K. (2013) Sulfur degassing at Erta Ale (Ethiopia) and Masaya (Nicaragua) volcanoes: Implications for degassing processes and oxygen fugacities of basaltic systems. Geochemistry, Geophysics, Geosystems, 14, 4076–4108.

Dickenson, M.P., and Hess, P.C. (1982) Redox equilibria and the structural role of iron in alumino-silicate melts. Contributions to Mineralogy and Petrology, 78, 352–357.

——— (1986) The structural role and homogeneous redox equilibria of iron in peraluminous, metaluminous and peralkaline silicate melts. Contributions to Mineralogy and Petrology, 92, 207–217.

Dufresne, C.D., King, P.L., Dyar, M.D., and Dalby, K.N. (2009) Effect of SiO_2, total FeO, Fe^{3+}/Fe^{2+}, and alkali elements in basaltic glasses on mid-infrared. American Mineralogist, 94, 1580–1590.

Dyar, M.D., McCanta, M., Breves, E., Carey, C.J., and Lanzirotti, A. (2016a) Accurate predictions of iron redox state in silicate glasses: A multivariate approach using X-ray absorption spectroscopy. American Mineralogist, 101, 744–747.

Dyar, M.D., Breves, E., Gunter, M.E., Lanzirotti, A., Tucker, J.M., Carey, C.J., Peel, S., Brown, E., Oberti, R., Lerotic, M., and others (2016b) Use of Multivariate Analysis for Synchrotron Micro-XANES Analysis of Iron Valence State in Amphiboles. American Mineralogist, 101, 1171–1189.

Fornari, D.J., Von Damm, K.L., Bryce, J.G., Cowen, J.P., Ferrini, V., Fundis, A., Lilley, M.D., Luther III, G.W., Mullineaux, L.S., and Perfit, M.R. (2012) The East Pacific Rise between 9 N and 10 N:

Twenty-five years of integrated, multidisciplinary oceanic spreading center studies. Oceanography, 25, 18–43.

Galoisy, L., Calas, G., and Arrio, M.A. (2001) High-resolution XANES spectra of iron in minerals and glasses: structural information from the pre-edge region. Chemical Geology, 174, 307–319.

Giuli, G., Paris, E., Mungall, J., Romano, C., and Dingwell, D. (2004) V oxidation state and coordination number in silicate glasses by XAS. American Mineralogist, 89, 1640–1646.

Hanson, B., and Jones, J.H. (1998) The systematics of Cr^{3+} and Cr^{2+} partitioning between olivine and liquid in the presence of spinel. American Mineralogist, 83, 669–684.

Helz, R.T., and Thornber, C.R. (1987) Geothermometry of Kilauea Iki lava lake, Hawaii. Bulletin of Volcanology, 49, 651–668.

Huebner, J.S., and Sato, M. (1970) The oxygen fugacity-temperature relationships of manganese oxide and nickel oxide buffers. American Mineralogist, 55, 934–952.

Jarosewich, E. (2002) Smithsonian Microbeam Standards. Journal of Research of the National Institute of Standards and Technology, 107, 681–685.

Jarosewich, E., Nelen, J. a., and Norberg, J.A. (1980) Reference Samples for Electron Microprobe Analysis. Geostandards Newsletter, 4, 43–47.

Johnston, W.D. (1965) Oxidation□Reduction Equilibria in Molten Na_2O. $2SiO_2$ Glass. Journal of the American Ceramic Society, 48, 184–190.

Jurewicz, A.J.G., Williams, R.J., Le, L., Wagstaff, J., Lofgren, G., Lanier, A., Carter, W., and Roshko, A. (1993) Technical Update: Johnson Space Center system using a solid electrolytic cell in a remote

location to measure oxygen fugacities in CO/CO_2 controlled-atmosphere furnaces pp. 1–40. National Aeronautics and Space Administration, Washington, D.C.

Karner, J.M., Sutton, S.R., Papike, J.J., Shearer, C.K., Jones, J.H., and Newville, M. (2006) Application of a new vanadium valence oxybarometer to basaltic glasses from the Earth, Moon, and Mars. American Mineralogist, 91, 270–277.

Kelley, K.A., and Cottrell, E. (2009) Water and the oxidation state of subduction zone magmas. Science, 325, 605–607.

Keppler, H. (1992) Crystal field spectra and geochemistry of transition metal ions in silicate melts and glasses. The American mineralogist, 77, 62–75.

Kilinc, A., Carmichael, I.S.E., Rivers, M.L., and Sack, R.O. (1983) The ferric-ferrous ratio of natural silicate liquids equilibrated in air. Contributions to Mineralogy and Petrology, 83, 136–140.

King, P.L., Hervig, R.L., Holloway, J.R., Delaney, J.S., and Dyar, M.D. (2000) Partitioning of Fe^{3+}/Fe_{total} between amphibole and basanitic melt as a function of oxygen fugacity. Earth and Planetary Science Letters, 178, 97–112.

Kraft, S., Stümpel, J., Becker, P., and Kuetgens, U. (1996) High resolution x□ray absorption spectroscopy with absolute energy calibration for the determination of absorption edge energies. Review of Scientific Instruments, 67, 681–687.

Kress, V.C., and Carmichael, I.S. (1991) The compressibility of silicate liquids containing Fe_2O_3 and the effect of composition, temperature, oxygen fugacity and pressure on their redox states. Contributions to Mineralogy and Petrology, 108, 82–92.

Lanzirotti, A., Newville, M., Manoukian, L., and Lange, K. (2016) High-speed, coupled micro-beam XRD/XRF/XAFS mapping at GSECARS: APS beamline 13-ID-E. In Clay Mineral Society

Workshop Lecture Series: Filling the Gaps - From Microscopic Pore Structures to Transport Properties in Shales Vol. 21, pp. 53–64. Clay Mineral Society.

Mallmann, G., and O'Neill, H.S.C. (2009) The crystal/melt partitioning of V during mantle melting as a function of oxygen fugacity compared with some other elements (Al, P, Ca, Sc, Ti, Cr, Fe, Ga, Y, Zr and Nb). Journal of Petrology, 50, 1765–1794.

Marescotti, P., Vanko, D.A., and Cabella, R. (2000) From oxidizing to reducing alteration: Mineralogical variations in pillow basalts from the east flank, Juan de Fuca Ridge. In Proc. Ocean Drill. Program Sci. Results Vol. 168, pp. 119–136.

Mathez, E.A. (1984) Influence of degassing on oxidation states of basaltic magmas. Nature, 310, 371–375.

O'Neill, H.S.C., and Pownceby, M.I. (1993) Thermodynamic data from redox reactions at high temperatures. I. An experimental and theoretical assessment of the electrochemical method using stabilized zirconia electrolytes, with revised values for the Fe-"FeO", Co-CoO, Ni-NiO and Cu-Cu_2O oxygen buffers, and new data for the W-WO_2 buffer. Contributions to Mineralogy and Petrology, 114, 296–314.

Papike, J.J., Karner, J.M., and Shearer, C.K. (2005) Comparative planetary mineralogy: Valence state partitioning of Cr, Fe, Ti, and V among crystallographic sites in olivine, pyroxene, and spinel from planetary basalts. American Mineralogist, 90, 277–290.

Pedregosa, F., Varoquaux, G., Gramfort, A., Michel, V., Thirion, B., Grisel, O., Blondel, M., Prettenhofer, P., Weiss, R., and Dubourg, V. (2011) Scikit-learn: Machine learning in Python. Journal of Machine Learning Research, 12, 2825–2830.

Ravel, B., and Newville, M. (2005) ATHENA , ARTEMIS , HEPHAESTUS : data analysis for X-ray absorption spectroscopy using IFEFFIT. Journal of Synchrotron Radiation, 12, 537–541.

Righter, K., Sutton, S., Danielson, L., Pando, K., Schmidt, G., Yang, H., Berthet, S., Newville, M., Choi, Y., and Downs, R.T. (2011) The effect of fO□ on the partitioning and valence of V and Cr in garnet/melt pairs and the relation to terrestrial mantle V and Cr content. American Mineralogist, 96, 1278–1290.

Sack, R.O., Carmichael, I.S.E., Rivers, M., and Ghiorso, M.S. (1980) Ferric-ferrous equilibria in natural silicate liquids at 1 bar. Contributions to Mineralogy and Petrology, 75, 369–376.

Sato, M. (1978) Oxygen fugacity of basaltic magmas and the role of gas□forming elements. Geophysical Research Letters, 5, 447–449.

Sato, M., and Wright, T.L. (1966) Oxygen fugacities directly measured in magmatic gases. Science, 153, 1103–1105.

Schreiber, H.D. (1986) Redox processes in glass-forming melts. Journal of Non-Crystalline Solids, 84, 129–141.

Schreiber, H.D., Kochanowski, B.K., Schreiber, C.W., Morgan, A.B., Coolbaugh, M.T., and Dunlap, T.G. (1994) Compositional dependence of redox equilibria in sodium silicate glasses. Journal of Non-Crystalline Solids, 177, 340–346.

Sutton, S.R., Karner, J., Papike, J., Delaney, J.S., Shearer, C., Newville, M., Eng, P., Rivers, M., and Dyar, M.D. (2005) Vanadium K edge XANES of synthetic and natural basaltic glasses and application to microscale oxygen barometry. Geochimica et Cosmochimica Acta, 69, 2333–2348.

Sutton, S.R., Lanzirotti, A., Newville, M., Rivers, M.L., Eng, P., and Lefticariu, L. (2017) Spatially Resolved Elemental Analysis, Spectroscopy and Diffraction at the GSECARS Sector at the Advanced Photon Source. Journal of Environmental Quality, 46, 1158–1165.

Tibshirani, R. (1996) Regression Shrinkage and Selection via the Lasso. Journal of the Royal Statistical Society. Series B (Methodological), 58, 267–288.

Wegelin, J.A. (2000) A survey of Partial Least Squares (PLS) methods, with emphasis on the two-block case. University of Washington, Department of Statistics, Tech. Rep.

Wilke, M., Partzsch, G.M., Bernhardt, R., and Lattard, D. (2005) Determination of the iron oxidation state in basaltic glasses using XANES at the K-edge. Chemical Geology, 220, 143–161.

Wilson, S.A., and Taggart, J.E. (2000) Development of USGS microbeam reference materials for geochemical analysis. In 4th International Conference on the Analysis of Geological and Environmental Materials. 29th Aug.-1st Sep., Pont a Mousson, Lorraine, France p. 24.

Wong, J., Lytle, F.W., Messmer, R.P., and Maylotte, D.H. (1984) K-edge absorption spectra of selected vanadium compounds. Physical Review B, 30, 5596.

Wright, T.L., and Okamura, R.T. (1977) Cooling and crystallization of tholeiitic basalt, 1965 Makaopuhi lava lake, Hawaii. U.S. Govt. Publishing Office.

Zhang, H.L., Hirschmann, M.M., Cottrell, E., Newville, M., and Lanzirotti, A. (2016) Structural environment of iron and accurate determination of $Fe^{3+}/\Sigma Fe$ ratios in andesitic glasses by XANES and Mössbauer spectroscopy. Chemical Geology, 428, 48–58.

FIGURE CAPTIONS

Figure 1: Vanadium K edge XANES spectra for the 28 experimental glasses, color-coded as a function of their known fO_2 (relative to NNO buffer) at equilibration. The top panel shows all 28 glasses superimposed, while the following three panels show the Cottrell, Dufresne and Hanson and Jones suites respectively. All intensities are edge-step normalized, as described in the text. The bottom panel is annotated to indicate the energy positions of major spectral features observed within the spectra analyzed. These include, for example, the pre-edge feature from the dipole forbidden 1*s*→3*d* transition and the main edge and white line structure resulting from the dipole-allowed 1*s*→4*p* transition. Absorption features above the white line can be attributed to competing interactions from the transition to higher *np* states, shape resonances, and multiple scattering effects.

Figure 2: Vanadium K edge XANES spectra for natural basaltic glasses analyzed, color-coded as a function of their predicted fO_2 (relative to NNO buffer) using the Lasso calibration model (α = 0.0008). The top panel plots spectra measured from USGS BCR-2G and from NMNH A-99 (Makaopuhi Lava Lake, Hawaii) and VG-2 (Juan de Fuca Ridge) standard glasses. The middle panel plots spectra measured from a sample of pillow-rim basaltic glass dredged from the East Pacific Rise. The bottom panel plots spectra measured in a sequence of seven basaltic glasses collected on 12/30/2014 from an active lava flow near Pahoa at Kilauea (Hawaii).

Figure 3: Model results for PLS (at a value of q = 4) showing all the Vanadium K edge XANES spectra from experimental glasses (in black, intensity scaling shown on the left axis) with PLS coefficients superimposed (in blue, coefficient scaling shown on the right axis). Positive PLS coefficients are channels that are positively correlated with the channel being predicted and

negative ones are the reverse. This model results in an internal cross-validated RMSE of 0.53 with an R^2 value of 0.97.

Figure 4: Model results for Lasso with variable values of α. Superimposed are vanadium K edge XANES spectra from experimental glasses (black) and calculated Lasso coefficients, where α was set to 0.01 (orange, RMSE = 0.701), 0.001 (green, RMSE = 0.362) and 0.0001 (purple, RMSE = 0.077). Spectral intensity scaling is shown on the left axis, while coefficient scaling is shown on the right axis.

Figure 5: Comparison of the experimentally determined NNO relative fO_2 values for experimental glasses to the Lasso predicted NNO relative fO_2. Symbols are scaled to the magnitude of the RMSE values (error bars) for predicted values, α=0.01 (blue), α=0.001 (red), α=0.0001 (black). The regression lines for each model are also shown.

Figure 6: Plots of the calculated T-fO_2 relationship for vanadium redox pairs V^{3+}/V^{2+} (olive), V^{4+}/V^{3+} (red) and V^{5+}/V^{4+} (green) in a cooling sodium disilicate melt (calculated using equations from Borisov 2013), compared to the calculated trend for the NNO buffer (dashed blue line, using O'Neill and Pownceby 1993). This is calculated between 980°C-1280°C, using a starting point of T = 1553K, fO_2 = -6.68 and shows that the trend of the V^{4+}/V^{3+} couple is almost identical to the slope of the NNO buffer.

Figure 7: Comparison of V (left panels) and Fe (right panels) K-edge XANES for experimental glasses equilibrated at similar nominal fO_2 conditions. The top two panels show the measured

spectra for the entire Hanson and Jones FAD suite of glasses. Both elements display systematic increases in valence as a function of increasing fO_2. The following panels compare spectra from FAD suite (in blue) to Cottrell or Dufresne suite glasses (natural basaltic starting materials, in red) equilibrated at similar nominal fO_2's of ~ NNO-3.3, NNO-0.7, and NNO+1.8. Whereas there is good agreement between the measured V spectroscopic features, Fe is present in a higher valence state in the FAD glasses at a given fO_2 relative to what is measured in glasses synthesized from natural basaltic materials.

Figure 8: SEM photomicrographs (left), V K-edge XANES (upper right) and Fe K-edge XANES (lower right) from basaltic glasses collected from an active lava flow at Kilauea. SEM photomicrographs of polished glass chips are annotated with their collection distance downflow in km. Samples consist of ~75-90% glass with small amounts of crystalline pyroxene and plagioclase. Normalized V XANES and Fe XANES spectra for each sample are shown, color-coded by their collection distance downflow in km. The mean predicted fO_2 for the seven samples based on the V oxybarometry (Lasso $\alpha = 0.0008$) is NNO-1.15 ±0.19 (1σ) and based on the Fe oxybarometry is NNO-1.08 ±0.20 (1σ).

Figure 9: Plane-light photomicrograph with superimposed FeKα X-ray fluorescence map (left), V K-edge XANES (upper right) and Fe K-edge XANES (lower right) from a sample of pillow basalt glass dredged from the East Pacific Rise. In the superimposed FeKα X-ray fluorescence grayscale map, areas with the highest Fe fluorescence are scaled as white and low Fe intensities as black. A 1 mm scale bar is shown in the lower left corner of the photomicrograph. The points selected for XANES analysis are annotated in yellow, extending ~5.5 mm into the pillow from

This is a preprint, the final version is subject to change, of the American Mineralogist (MSA)
Cite as Authors (Year) Title. American Mineralogist, in press.
DOI: https://doi.org/10.2138/am-2018-6319

its quenched surface (left side of the sample). Normalized V XANES and Fe XANES spectra for each analysis point are shown, color-coded by relative distance in mm from the quenched surface. The mean predicted fO_2 for all analytical points based on the V oxybarometry (Lasso α = 0.0008) is NNO-6.62 ±0.48 (1σ) and based on the Fe oxybarometry is NNO-2.54 ±0.19 (1σ). However, V XANES shows clear evidence for oxidation approaching the quenched surface which is not detectable within uncertainty using Fe XANES, reflecting the higher sensitivity of V oxybarometry is highly reduced basaltic glasses.

This is a preprint, the final version is subject to change, of the American Mineralogist (MSA)
Cite as Authors (Year) Title. American Mineralogist, in press.
DOI: https://doi.org/10.2138/am-2018-6319

Figure 1

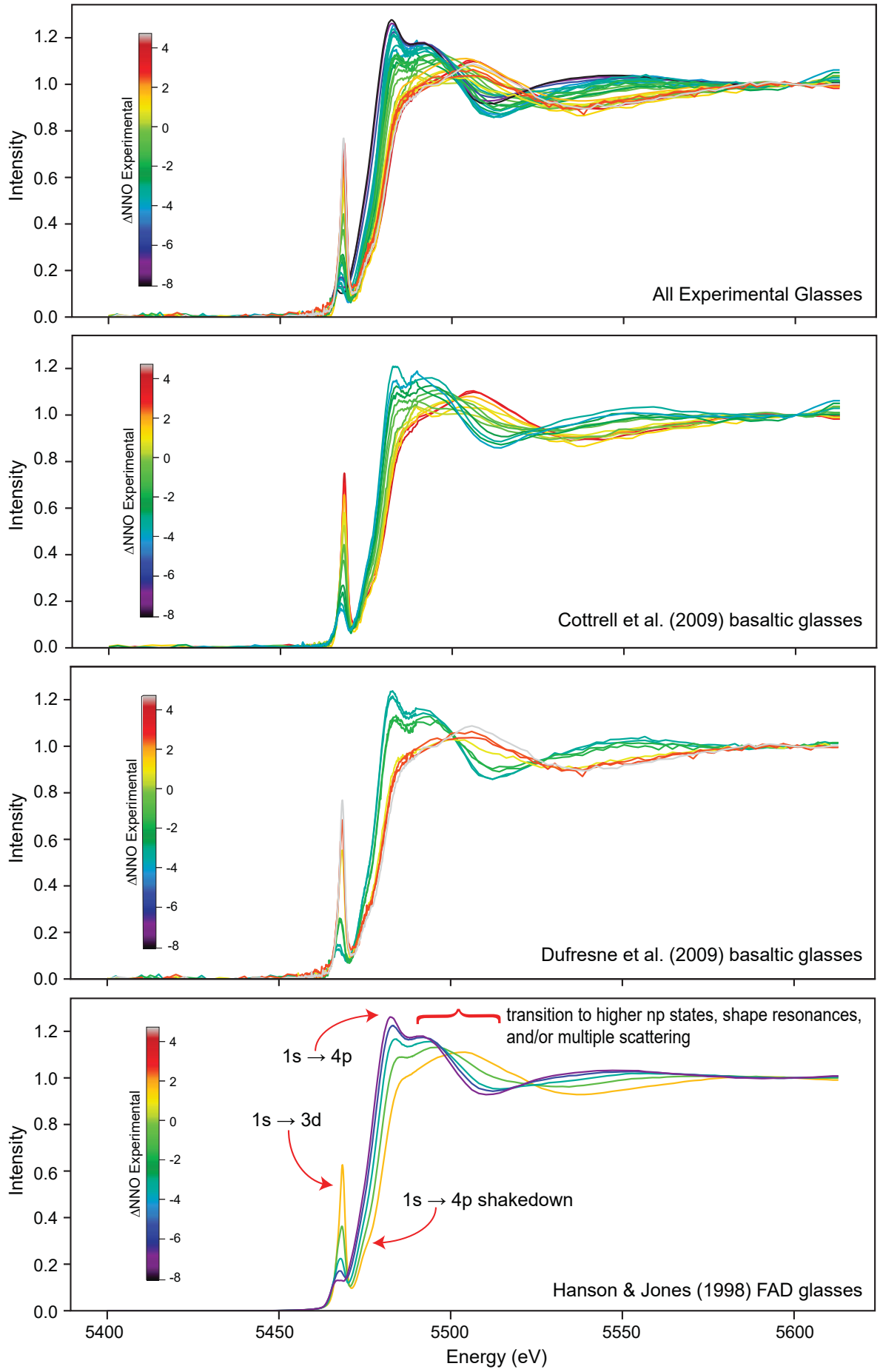

This is a preprint, the final version is subject to change, of the American Mineralogist (MSA)
Cite as Authors (Year) Title. American Mineralogist, in press.
DOI: https://doi.org/10.2138/am-2018-6319

Figure 2

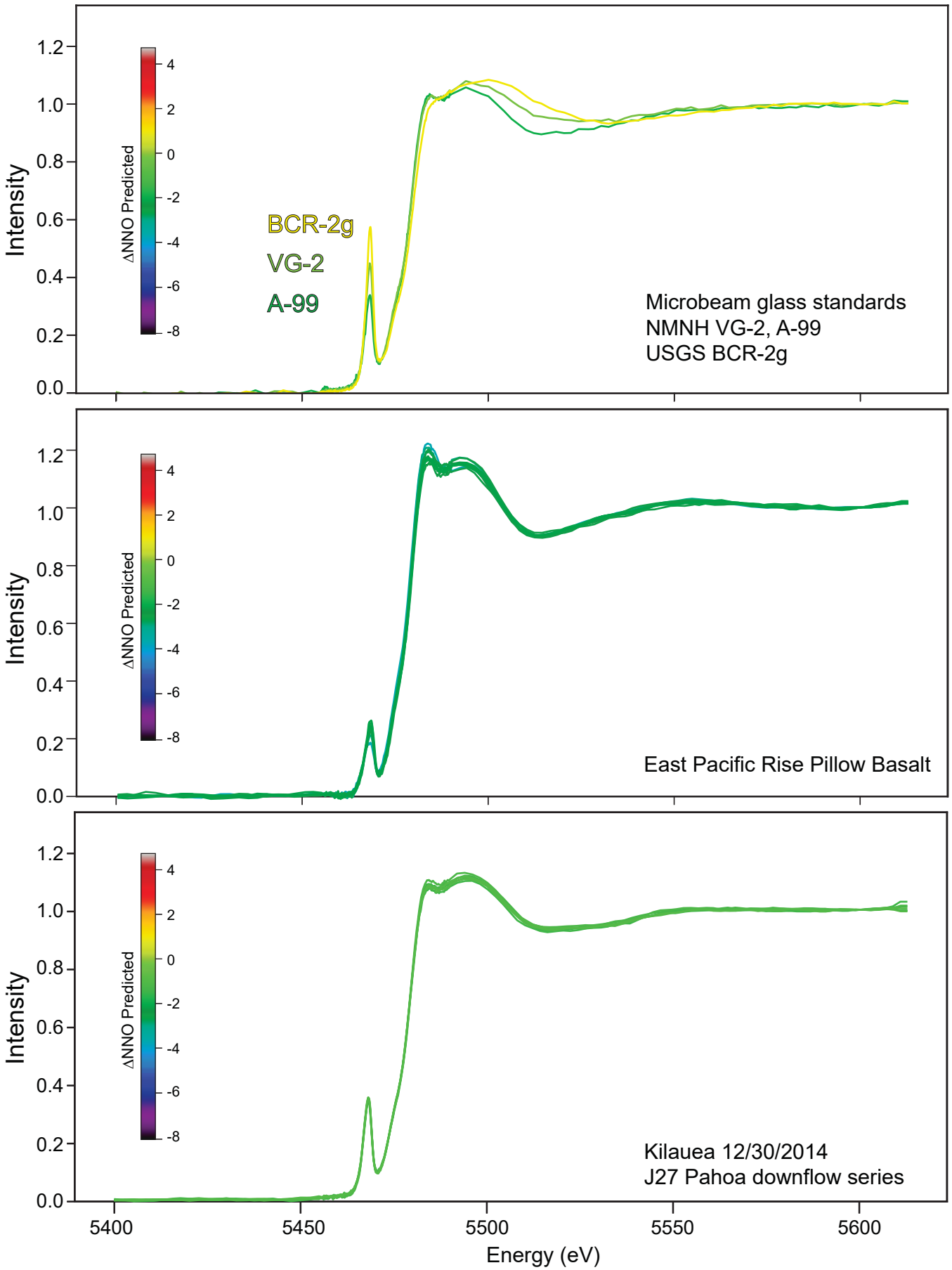

This is a preprint, the final version is subject to change, of the American Mineralogist (MSA)
Cite as Authors (Year) Title. American Mineralogist, in press.
DOI: https://doi.org/10.2138/am-2018-6319

Figure 3

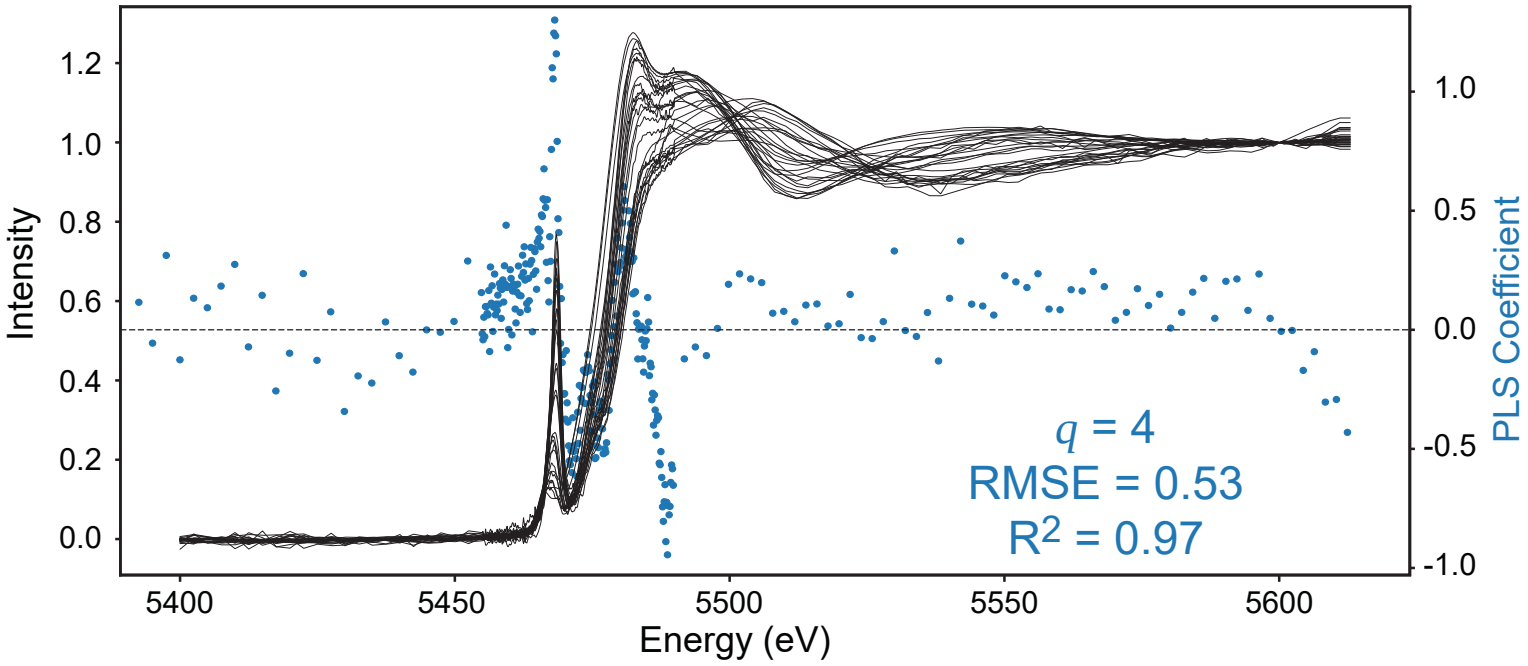

This is a preprint, the final version is subject to change, of the American Mineralogist (MSA)
Cite as Authors (Year) Title. American Mineralogist, in press.
DOI: https://doi.org/10.2138/am-2018-6319

Figure 4

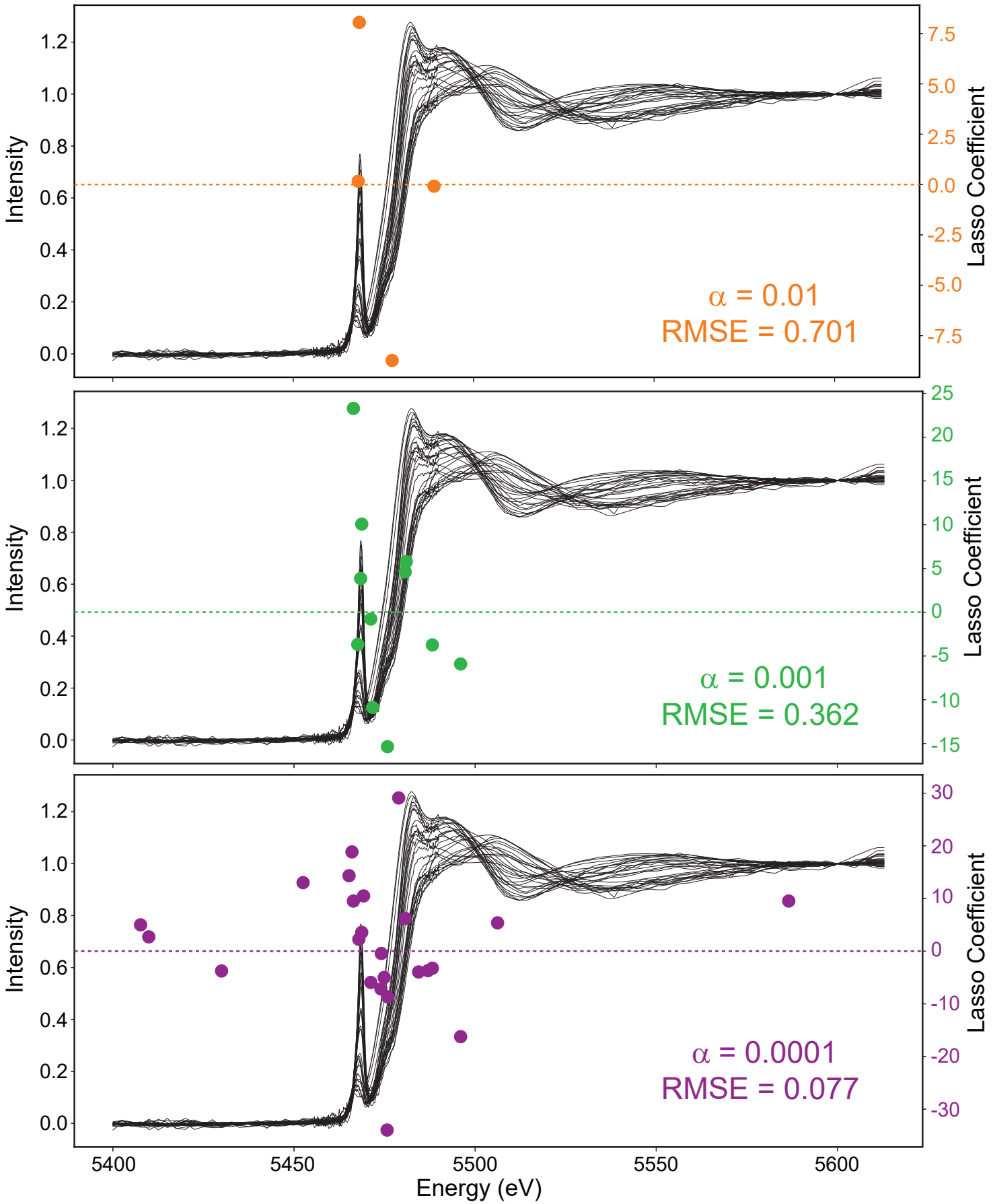

This is a preprint, the final version is subject to change, of the American Mineralogist (MSA)
Cite as Authors (Year) Title. American Mineralogist, in press.
DOI: https://doi.org/10.2138/am-2018-6319

Figure 5

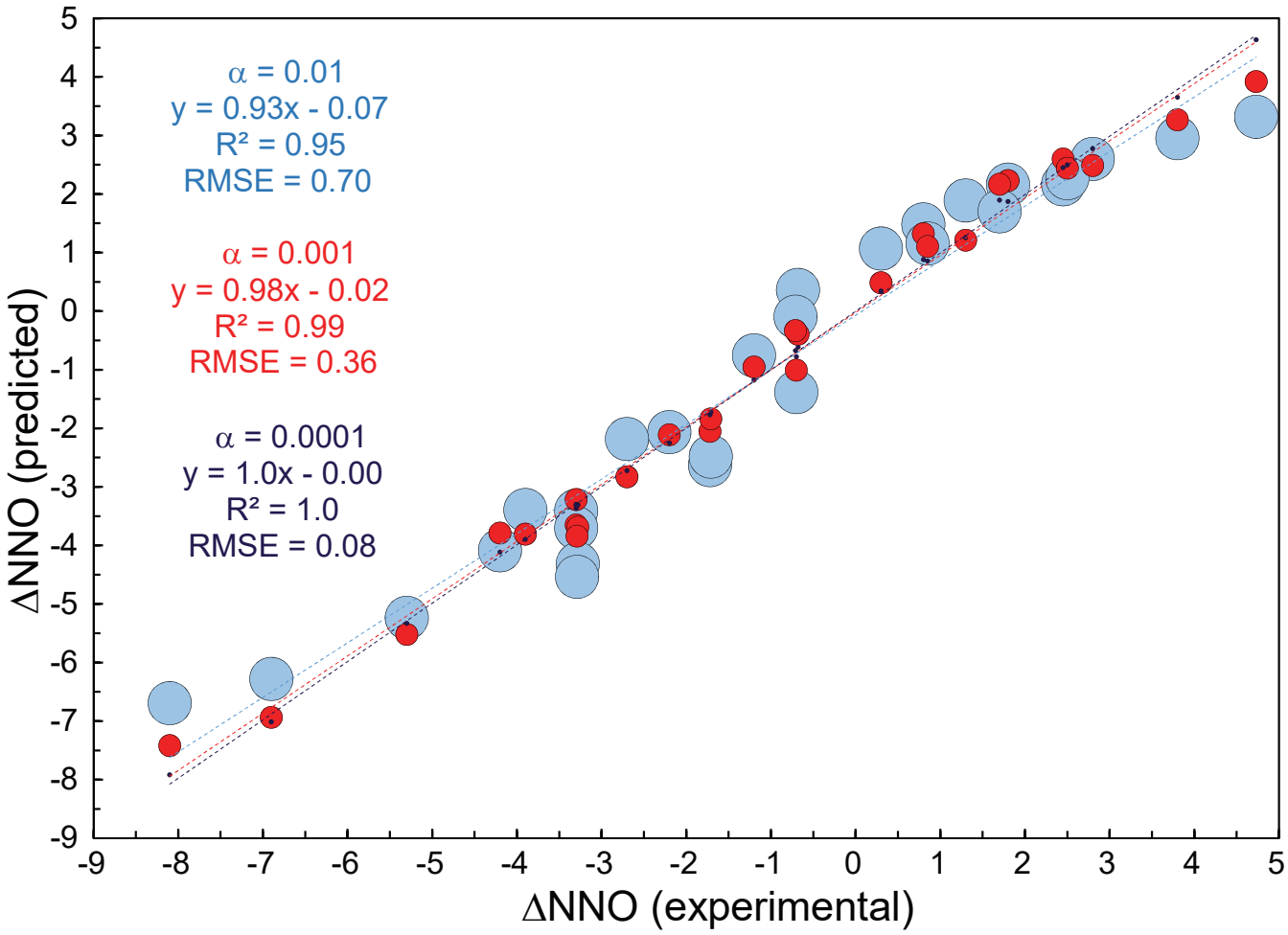

This is a preprint, the final version is subject to change, of the American Mineralogist (MSA)
Cite as Authors (Year) Title. American Mineralogist, in press.
DOI: https://doi.org/10.2138/am-2018-6319

Figure 6

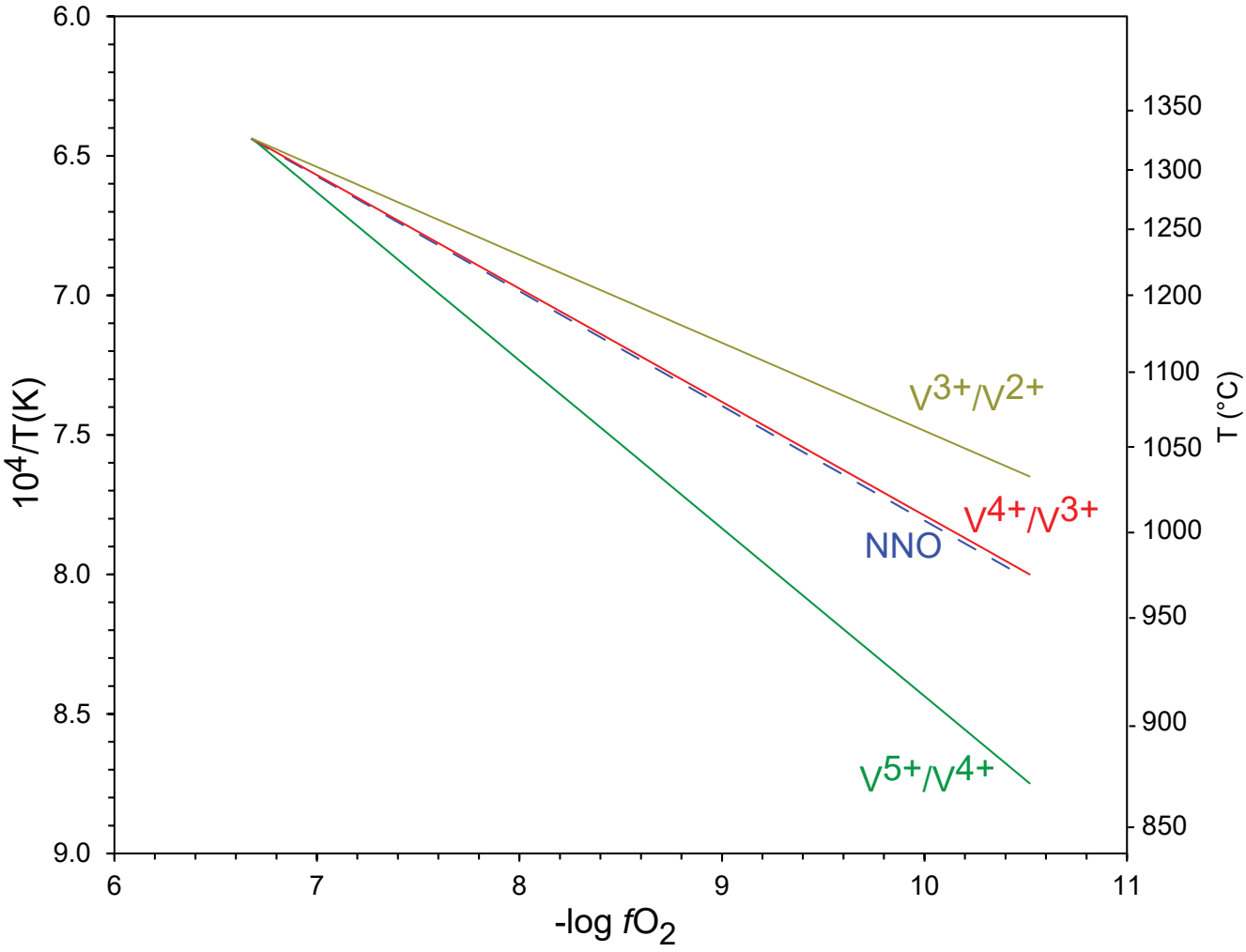

This is a preprint, the final version is subject to change, of the American Mineralogist (MSA)
Cite as Authors (Year) Title. American Mineralogist, in press.
DOI: https://doi.org/10.2138/am-2018-6319

Figure 7

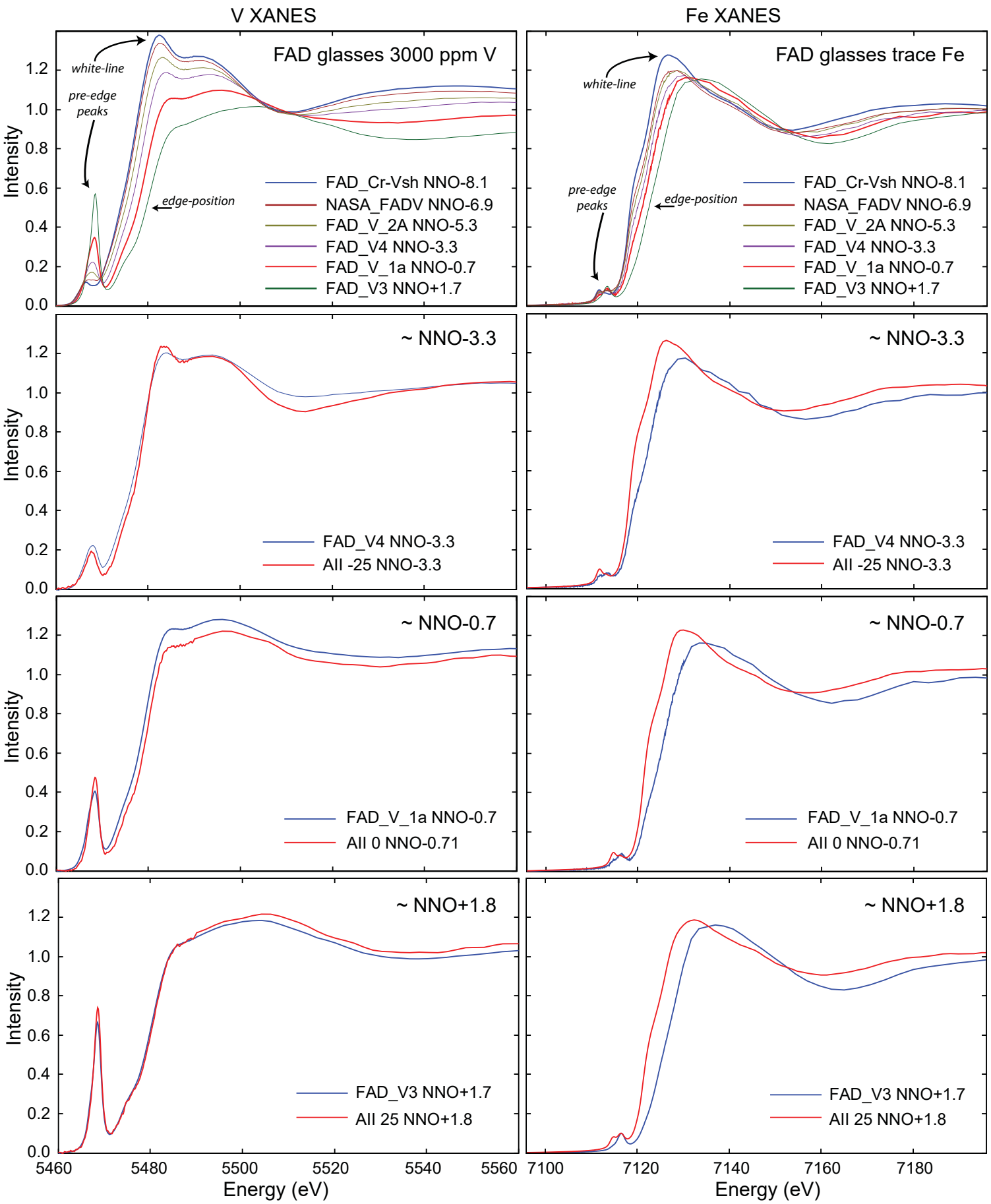

This is a preprint, the final version is subject to change, of the American Mineralogist (MSA)
Cite as Authors (Year) Title. American Mineralogist, in press.
DOI: https://doi.org/10.2138/am-2018-6319

Figure 8

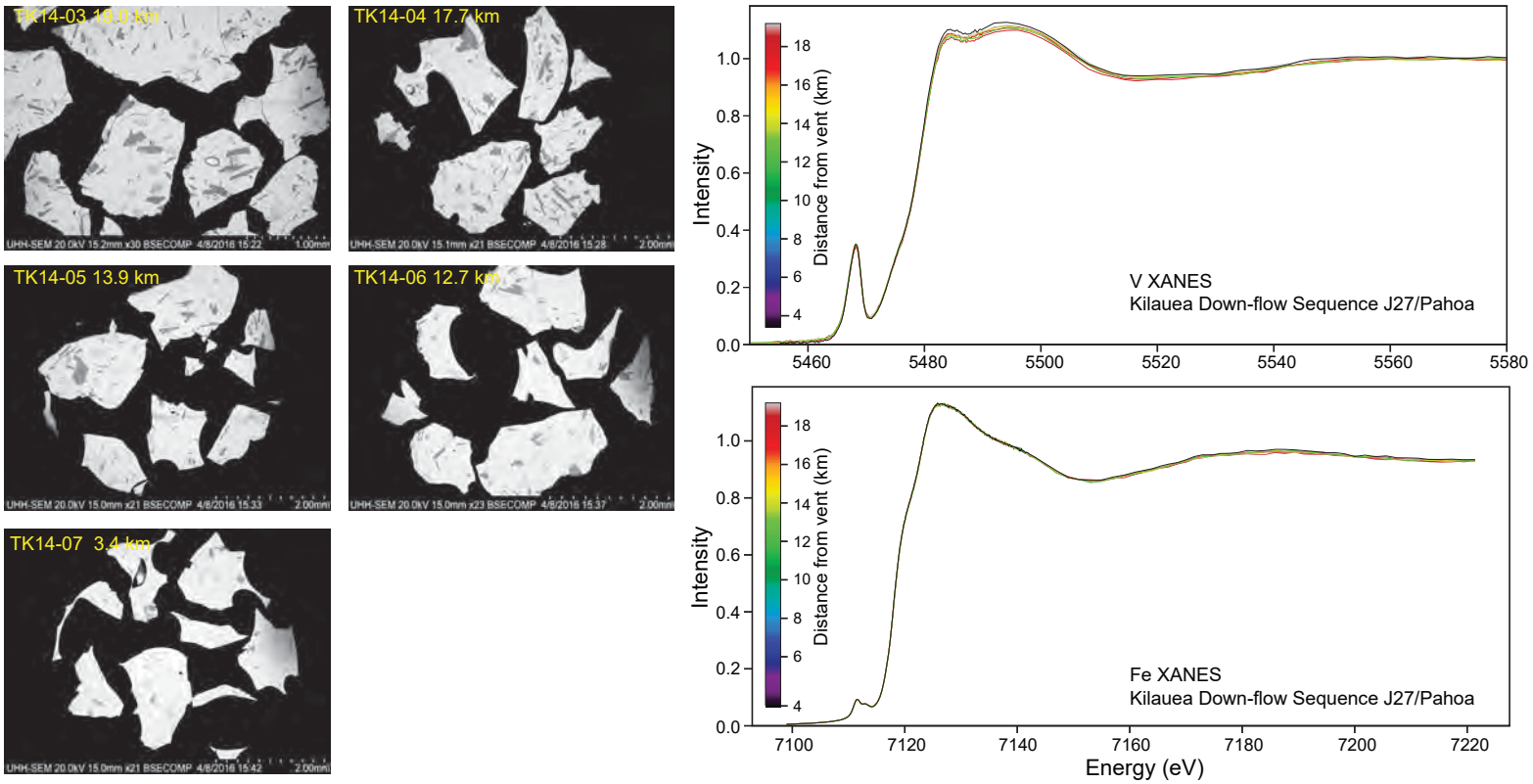

This is a preprint, the final version is subject to change, of the American Mineralogist (MSA)
Cite as Authors (Year) Title. American Mineralogist, in press.
DOI: https://doi.org/10.2138/am-2018-6319

Figure 9

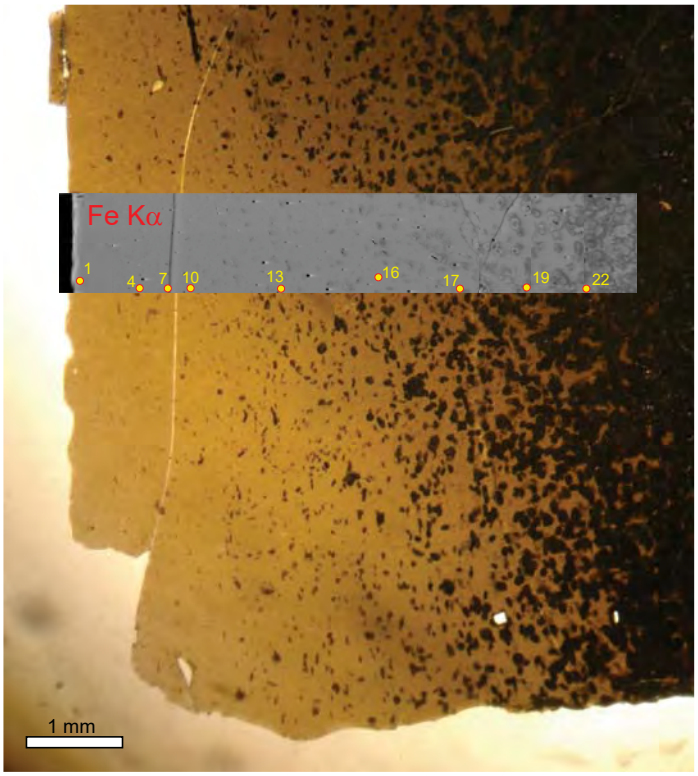

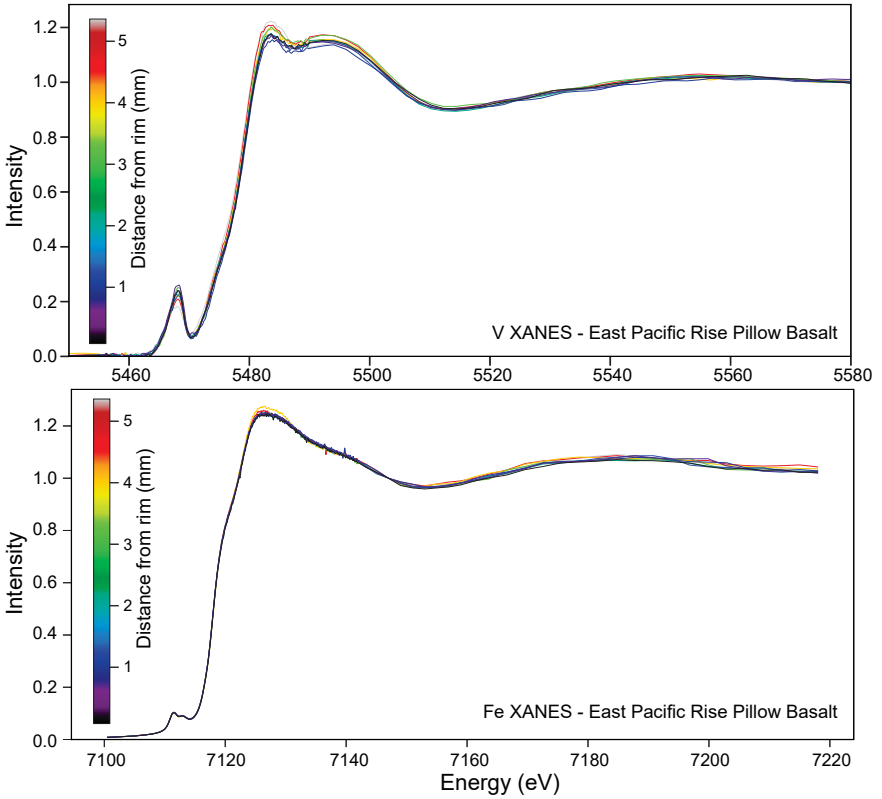

This is a preprint, the final version is subject to change, of the American Mineralogist (MSA)
Cite as Authors (Year) Title. American Mineralogist, in press.
DOI: https://doi.org/10.2138/am-2018-6319

Table 1: System compositions and equilibration conditions for experimental glasses

	SiO_2	TiO_2	Al_2O_3	$FeO_{(T)}$	MnO	MgO	CaO	Na_2O	K_2O	P_2O_5	T (°C)	Ref.
Hanson FAD	46.1	0.0	12.0	0.0	0.0	27.9	13.6	0.0	0.0	nd	1320	a
Cottrell LW	49.4	1.9	17.2	10.2	nd	6.1	8.8	3.2	1.5	1.1	1350	b
Cottrell AII	50.8	1.7	16.1	9.5	nd	7.4	11.2	2.8	0.2	0.1	1350	b
Dufresne												
NNO-3 Re	51.1	2.6	11.6	11.3	0.2	10.0	10.4	0.4	0.2	0.2	1415	c
NNO-3 dPt	54.9	2.8	12.5	6.9	0.2	10.6	11.2	0.7	0.3	0.1	1415	c
NNO-1.5 Re	51.5	2.7	11.9	11.3	0.2	9.9	10.7	0.1	0.0	0.2	1417	c
NNO-1.5 dPt	51.4	2.7	12.1	10.4	0.2	9.9	10.7	1.5	0.4	0.2	1415	c
NNO+1 Pt	50.1	2.7	11.9	9.7	0.2	9.9	10.6	1.8	0.5	0.2	1416	c
NNO+3 Pt	50.3	2.6	11.7	10.8	0.2	9.7	10.5	1.9	0.5	0.2	1416	c
NNO+3 dPt	49.7	2.6	12.0	12.7	0.2	9.6	10.2	1.9	0.5	0.2	1410	c
NNO+5 Pt	50.2	2.7	11.7	11.0	0.2	9.7	10.4	1.9	0.5	0.2	1415	c

(a) Hanson and Jones 1998 (b) Cottrell et al. 2009 (c) Dufresne et al. 2009

This is a preprint, the final version is subject to change, of the American Mineralogist (MSA)
Cite as Authors (Year) Title. American Mineralogist, in press.
DOI: https://doi.org/10.2138/am-2018-6319

Table 2: Experimental oxygen fugacities of synthetic glasses used to train MVA models, predicted V XANES ΔNNO, measured $Fe^{3+}/\Sigma Fe$.

	log(fO_2)	ΔNNO experimental	ΔNNO predicted PLS	ΔNNO predicted LASSO	$Fe^{3+}/\Sigma Fe$ [a]
Hanson FAD					
FAD_V3	-4.55	1.70	2.18 (0.53)	2.21 (0.33)	0.75
FAD_V_1a	-7.05	-0.70	-0.96 (0.53)	-0.98 (0.33)	0.52
FAD_V4	-9.55	-3.30	-3.62 (0.53)	-3.64 (0.33)	0.33
FAD_V_2A	-11.55	-5.30	-5.57 (0.53)	-5.53 (0.33)	0.27
NASA_FADV	-13.20	-6.90	-7.04 (0.53)	-6.98 (0.33)	0.15
FAD_Cr-Vsh	-15.30	-8.10	-7.54 (0.53)	-7.45 (0.33)	0.08
Cottrell					
AII_45	-2.20	3.80	3.27 (0.53)	3.29 (0.33)	0.61
AII_35	-3.22	2.80	2.64 (0.53)	2.48 (0.33)	0.48
AII_25	-4.25	1.80	1.83 (0.53)	2.21 (0.33)	0.36
LW_20	-4.73	1.30	1.45 (0.53)	1.22 (0.33)	0.30
AII_15	-5.24	0.80	0.73 (0.53)	1.29 (0.33)	0.25
LW_10	-5.72	0.30	0.38 (0.53)	0.43 (0.33)	0.24
LW_0	-6.68	-0.68	-0.53 (0.53)	-0.42 (0.33)	0.16
AII_0	-6.71	-0.71	-0.61 (0.53)	-0.42 (0.33)	0.15
AII_-05	-7.20	-1.20	-1.06 (0.53)	-1.03 (0.33)	0.14
AII_-15	-8.22	-2.20	-2.09 (0.53)	-2.15 (0.33)	0.09
LW_-20	-8.72	-2.70	-2.78 (0.53)	-2.84 (0.33)	0.09
AII_-25	-9.31	-3.30	-3.14 (0.53)	-3.24 (0.33)	0.05
LW_-30	-9.86	-3.90	-4.07 (0.53)	-3.78 (0.33)	0.04
AII_-35	-10.19	-4.20	-3.93 (0.53)	-3.81 (0.33)	0.04
Dufresne					
NNO+5 Pt	-0.68	4.73	4.73 (0.53)	4.03 (0.33)	0.54
NNO+3 dPt	-2.95	2.50	2.66 (0.53)	2.48 (0.33)	0.50
NNO+3 Pt	-2.95	2.45	2.68 (0.53)	2.58 (0.33)	0.53
NNO+1 Pt	-4.55	0.85	0.61 (0.53)	1.05 (0.33)	0.35
NNO-1.5 dPt	-7.12	-1.71	-1.73 (0.53)	-1.83 (0.33)	0.07
NNO-1.5 Re	-7.11	-1.72	-1.69 (0.53)	-1.99 (0.33)	0.09
NNO-3 dPt	-8.70	-3.29	-3.23 (0.53)	-3.72 (0.33)	0.07
NNO-3 Re	-8.69	-3.28	-3.73 (0.53)	-3.62 (0.33)	0.05

(a) The $Fe^{3+}/\Sigma Fe$ value reported for the Cottrell et al. (2009) and Dufresne et al. (2009) glasses are reported in the respective references. For these the values in black were measured by Mössbauer spectroscopy and the orange values were predicted from Fe XANES spectroscopy. The values reported for the Hanson and Jones (1998) suite are predicted based on the Fe XANES measurements in this manuscript.

Table 3: Predicted oxygen fugacities of microbeam standard glasses

	V ΔNNO predicted[a]
BCR-2G	1.08 (0.33)
VG-2	-0.08 (0.33)
A-99	-1.28 (0.33)

(a) Calculated oxygen fugacity relative to NNO buffer using vanadium LASSO MVA model, $\alpha = 0.0008$.

This is a preprint, the final version is subject to change, of the American Mineralogist (MSA)
Cite as Authors (Year) Title. American Mineralogist, in press.
DOI: https://doi.org/10.2138/am-2018-6319

Table 4: Sampling distances, predicted oxygen fugacities and measured Fe valence of Kilauea glasses

	Distance from vent (km)	V ΔNNO predicted [a]	$Fe^{3+}/\Sigma Fe$ [b]	$Fe^{3+}/\Sigma Fe$ predicted ΔNNO [c]
HVO_TK14-01	18.7	-0.96 (0.33)	0.15 (0.04)	-0.8 (0.6)
HVO_TK14-02	17.6	-1.34 (0.33)	0.14 (0.04)	-0.9 (0.6)
HVO_TK14-03	19.2	-1.25 (0.33)	0.13 (0.04)	-1.1 (0.6)
HVO_TK14-04	17.7	-1.41 (0.33)	0.13 (0.04)	-1.1 (0.6)
HVO_TK14-05	13.9	-0.98 (0.33)	0.13 (0.04)	-1.1 (0.6)
HVO_TK14-06	12.7	-0.97 (0.33)	0.12 (0.04)	-1.3 (0.6)
HVO_TK14-07	3.4	-1.13 (0.33)	0.12 (0.04)	-1.3 (0.6)

(a) Calculated oxygen fugacity relative to NNO buffer using vanadium LASSO MVA model, $\alpha = 0.0008$.

(b) Calculated $Fe^{3+}/\Sigma Fe$ from Fe XANES data using Dyar et al. (2016a) MVA model, PLS with $q = 4$. Errors on prediction of $\%Fe^{3+}$ in glasses using the Dyar et al. (2016a) MVA model are quoted as ± 3.6 $\%Fe^{3+}$.

(c) Calculated oxygen fugacity relative to NNO buffer using Kress and Carmichael (1991) equation, calculated $Fe^{3+}/\Sigma Fe$, major element composition, estimated liquidus temperature (1130°C) and assuming 1 bar pressure . Errors based on assumed $Fe^{3+}/\Sigma Fe$ uncertainty.

This is a preprint, the final version is subject to change, of the American Mineralogist (MSA)
Cite as Authors (Year) Title. American Mineralogist, in press.
DOI: https://doi.org/10.2138/am-2018-6319

Table 5: Sampling distances, predicted oxygen fugacities and measured Fe valence of East Pacific Rise pillow glass

	Distance from rim (mm)	V ΔNNO predicted [a]	$Fe^{3+}/\Sigma Fe$ [b]	$Fe^{3+}/\Sigma Fe$ predicted ΔNNO [c]	Fe pre-edge centroid (eV) [d]
EPR2-1	0.08	-2.67 (0.33)	0.067 (0.036)	-2.8 (1.0)	7111.91 (0.01)
EPR2-4	0.71	-2.09 (0.33)	0.069 (0.036)	-2.7 (1.0)	7111.94 (0.01)
EPR2-7	1.01	-2.19 (0.33)	0.072 (0.036)	-2.6 (1.0)	7111.94 (0.01)
EPR2-10	1.24	-2.31 (0.33)	0.076 (0.036)	-2.5 (1.0)	7111.93 (0.01)
EPR2-13	2.17	-2.45 (0.33)	0.080 (0.036)	-2.4 (1.0)	7111.93 (0.01)
EPR2-16	3.20	-2.56 (0.33)	0.082 (0.036)	-2.3 (1.0)	7111.95 (0.01)
EPR2-17	4.04	-2.68 (0.33)	0.076 (0.036)	-2.5 (1.0)	7111.94 (0.01)
EPR2-19	4.74	-2.90 (0.33)	0.066 (0.036)	-2.8 (1.0)	7111.93 (0.01)
EPR2-22	5.36	-3.72 (0.33)	0.080 (0.036)	-2.4 (1.0)	7111.94 (0.01)

(a) Calculated oxygen fugacity relative to NNO buffer using vanadium LASSO MVA model, $\alpha = 0.0008$.

(b) Calculated $Fe^{3+}/\Sigma Fe$ from Fe XANES data using Dyar et al. (2016a) MVA model, PLS with $q = 4$. Errors on prediction of $\%Fe^{3+}$ in glasses using the Dyar et al. (2016a) MVA model are quoted as ± 3.6 $\%Fe^{3+}$.

(c) Calculated oxygen fugacity relative to NNO buffer using Kress and Carmichael (1991) equation, calculated $Fe^{3+}/\Sigma Fe$, major element composition, and estimated liquidus (1200 °C) and pressure (250 bars). Errors based on assumed $Fe^{3+}/\Sigma Fe$ uncertainty.

(d) Fe XANES area weighted pre-edge energy.

Table 6: LASSO α = 0.0008 MVA model, energy channels and coefficients

Energy Channel (eV)	Coefficient
5459.5	2.02433
5466.4	27.9168
5467.6	-5.66453
5468.4	3.49525
5468.7	11.5190
5471.2	-0.87365
5471.5	-13.1486
5475.8	-15.2376
5480.7	5.47529
5480.9	5.65545
5488.2	-2.66563
5496.0	-7.73172

This is a preprint, the final version is subject to change, of the American Mineralogist (MSA)
Cite as Authors (Year) Title. American Mineralogist, in press.
DOI: https://doi.org/10.2138/am-2018-6319

Table 7: Calculated Fe concentrations for FAD glasses

	Fe (ppm)
FAD_V3	591
FAD_V_1a	64
FAD_V4	47
FAD_V_2A	83
NASA_FADV	8600
FAD_Cr_Vsh	4400